
Chapter 8

Pulse Compression Radar

Michael R. Ducoff

Byron W. Tietjen

Lockheed Martin MS2

8.1 INTRODUCTION*

A pulse compression radar transmits a long pulse with pulsedwidth T and peak power P_p , which is coded using frequency or phase modulation to achieve a bandwidth B that is large compared to that of an uncoded pulse with the same duration.¹ The transmit pulsedwidth is chosen to achieve the single-pulse transmit energy, given by $E_{rl} = P_p T$, that is required for target detection or tracking. The received echo is processed using a pulse compression filter to yield a narrow compressed pulse response with a mainlobe width of approximately $1/B$ that does not depend on the duration of the transmitted pulse.

Figure 8.1 shows a block diagram of a basic pulse compression radar. The coded pulse is generated at a low power level in the waveform generator and amplified to the required peak transmit power using a power amplifier transmitter. The received signal is mixed to an intermediate frequency (IF) and amplified by the IF amplifier. The signal is then processed using a pulse compression filter that consists of a matched filter to achieve maximum signal-to-noise ratio (SNR). As discussed below, the matched filter is followed by a weighting filter if required for reduction of time sidelobes. The output of the pulse compression filter is applied to an envelope detector, amplified by the video amplifier, and displayed to an operator.

The ratio of the transmit pulsedwidth to the compressed pulse mainlobe width is defined as the pulse compression ratio. The pulse compression ratio is approximately $T/(1/B)$ or TB , where TB is defined as the time-bandwidth product of the waveform. Typically, the pulse compression ratio and time-bandwidth product are large compared to unity.

The use of pulse compression provides several performance advantages. The increased detection range capability of a long-pulse radar system is achieved with pulse compression while retaining the range resolution capability of a radar that uses a narrow uncoded pulse. The required transmitted energy can be established by

* The authors would like to acknowledge the use of material previously prepared by Edward C. Farnett and George H. Stevens for the "Pulse Compression Radar" chapter in the second edition of the *Radar Handbook* (1990), edited by Merrill I. Skolnik.

8.1

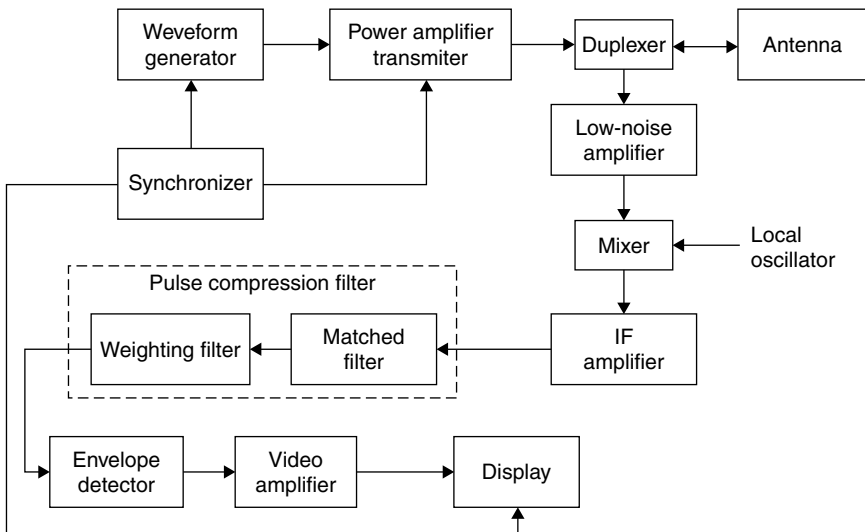


FIGURE 8.1 Block diagram of a basic pulse compression radar

increasing the waveform pulselength without exceeding constraints on transmitter peak power. The average power of the radar may be increased without increasing the pulse repetition frequency (PRF) and, hence, decreasing the radar's unambiguous range. In addition, the radar is less vulnerable to interfering signals that differ from the coded transmitted signal.

The mainlobe of the compressed pulse at the output of the matched filter has time, or range, sidelobes that occur within time intervals of duration T , before and after the peak of the peak of the compressed pulse. The time sidelobes can conceal targets, which would otherwise be resolved using a narrow uncoded pulse. In some cases, such as phase-coded waveforms or nonlinear frequency modulation waveforms, matched filter processing alone achieves acceptable time sidelobe levels. However, for the case of a linear frequency modulation waveform, the matched filter is generally followed by a weighting filter to provide a reduction in time sidelobe levels. In this case, the weighting filter results in a signal-to-noise ratio loss compared to that of matched filter processing alone.

8.2 PULSE COMPRESSION WAVEFORM TYPES

The following sections describe the characteristics of the linear and nonlinear frequency modulation waveforms, phase-coded waveforms, and time-frequency coded waveforms. The application of surface acoustic wave (SAW) devices for linear frequency modulation (LFM) waveform pulse compression is discussed. Waveform signal analysis techniques, matched filter properties, and the waveform autocorrelation and ambiguity function definitions used are summarized in the Appendix at the end of this chapter.

Linear Frequency Modulation.^{1,2} The linear frequency modulation, or chirp, waveform has a rectangular amplitude modulation with pulsewidth T and a linear frequency modulation with a swept bandwidth B applied over the pulse. The time-bandwidth product of the LFM waveform is equal to TB , where TB is the product of pulsewidth and swept bandwidth. The 3-dB width of the compressed pulse at the output of the matched filter is $\tau_3 = 0.886/B$, for large values of time-bandwidth product. The peak time sidelobe level of the compressed pulse is -13.2 dB.

As discussed in Section 8.1, a frequency-domain weighting filter is generally required following the matched filter to provide reduced time sidelobe levels, at the cost of reduced SNR and an increase in the width of the compressed pulse. As an example, the use of 40-dB Taylor weighting reduces the peak time sidelobe level from -13.2 dB to -40 dB and introduces a 1.15 dB loss in SNR. The 3-dB width of the compressed pulse with weighting increases from $\tau_3 = 0.886/B$ to $\tau_3 = 1.25/B$.

The LFM waveform has a knife-edge ambiguity function with contours that are approximately elliptical with a major axis defined by the line $v = \alpha\tau$, where $\alpha = \pm B/T$ is the LFM slope. This property introduces range-doppler coupling at the matched filter output causing the matched filter output peak to occur earlier in time for a target with a positive doppler frequency compared to a stationary target at the same range, assuming a positive linear frequency modulation slope and later in time for a negative slope.

The compressed pulse shape and SNR are tolerant to doppler shift for the LFM waveform. As a result, it is not necessary to implement multiple matched filters to cover the range of expected target doppler shifts.

LFM Waveform Definition. The LFM waveform is a single-pulse bandpass signal defined as

$$x(t) = A \operatorname{rect}(t/T) \cos[2\pi f_0 t + \pi\alpha t^2] \quad (8.1)$$

where T is the pulsewidth, f_0 is the carrier frequency, α is the LFM slope, and the rect function is defined as

$$\operatorname{rect}(x) = \begin{cases} 1, & |x| < 1/2 \\ 0, & |x| > 1/2 \end{cases} \quad (8.2)$$

The LFM slope is given by $\alpha = \pm B/T$, where the plus sign applies for a positive LFM slope (termed an *up-chirp*) and the minus sign for a negative LFM slope (a *down-chirp*). The amplitude modulation is $a(t) = A \operatorname{rect}(t/T)$ and the phase modulation is a quadratic function of time:

$$\phi(t) = \pi\alpha t^2 \quad (8.3)$$

The frequency modulation, defined as the instantaneous frequency deviation from the carrier frequency f_0 , is expressed in terms of the phase modulation by

$$f_i(t) = \frac{1}{2\pi} \frac{d\phi}{dt} \quad (8.4)$$

The frequency modulation for an LFM waveform is linear with slope equal to α

$$f_i(t) = \alpha t = \pm(B/T)t, \quad |t| \leq T/2 \quad (8.5)$$

where the plus sign applies for a positive LFM slope and the minus sign for a negative slope. The complex envelope of the LFM waveform is expressed in terms of the amplitude and phase modulation functions as

$$u(t) = A \operatorname{rect}(t/T) e^{j\pi\alpha t^2}$$

Figure 8.2 shows an example of an LFM bandpass signal with a pulsewidth $T = 10 \mu s$, swept bandwidth $B = 1 \text{ MHz}$ and time-bandwidth product equal to $\text{TB} = 10$. The LFM slope is $B/T = 0.1 \text{ MHz}/\mu s$. The instantaneous frequency of the LFM waveform varies between 1.5 and 2.5 MHz over the pulse duration, as indicated by the reduction in the spacing of successive positive-going zero crossings of the signal.[†]

LFM Waveform Spectrum.^{1,2,3} The spectrum of the LFM waveform has a significant amplitude variation versus frequency for small time-bandwidth products. For large values of time-bandwidth product, the magnitude of the spectrum approaches $\operatorname{rect}(f/B)$

$$u(t) = \frac{1}{\sqrt{T}} \operatorname{rect}(t/T) e^{j\pi\alpha t^2} \quad (8.6)$$

$$|U(f)| \approx \operatorname{rect}(f/B) \text{ for } \text{TB} \gg 1$$

The LFM spectrum is expressed in terms of the complex Fresnel integral, and the amplitude variation present for low values of TB is termed the *Fresnel ripple*.

LFM Waveform Ambiguity Function. The waveform autocorrelation function and ambiguity function for an LFM waveform are given by

$$\chi_u(\tau, f_d) = [1 - |\tau/T|] \operatorname{sinc}[(f_d - \alpha\tau)T(1 - |\tau/T|)] \operatorname{rect}(\tau/2T) e^{-j\pi f_d \tau} \quad (8.7)$$

$$\Psi_u(\tau, f_d) = [1 - |\tau/T|]^2 \operatorname{sinc}^2[(f_d - \alpha\tau)T(1 - |\tau/T|)] \operatorname{rect}(\tau/2T) \quad (8.8)$$

where the sinc function is defined as

$$\operatorname{sinc}(x) = \sin(\pi x)/(\pi x)$$

The matched filter time response for a target with doppler shift f_d is obtained by the substitution $\tau = -t$ in the autocorrelation function:

$$y(t) = \chi_u(-t, f_d) = [1 - |t/T|] \operatorname{sinc}[(f_d + \alpha t)T(1 - |t/T|)] \operatorname{rect}(t/2T) e^{j\pi f_d t} \quad (8.9)$$

LFM Range-doppler Coupling. The LFM waveform exhibits range-doppler coupling which causes the peak of the compressed pulse to shift in time by an amount proportional to the doppler frequency. The peak occurs earlier in time at $t = -f_d T/B$ for a positive LFM slope, compared to peak response for a stationary target. The peak of the ambiguity function is shifted to $\tau = f_d T/B$ for a positive LFM slope.

Time Delay and Range Resolution Widths. The time-delay resolution width is equal to the width of the ambiguity function at a specified level relative to the peak value.

[†] Low values of carrier frequency and time-bandwidth product have been used to illustrate the variation of instantaneous frequency over the pulse in Figure 8.2.

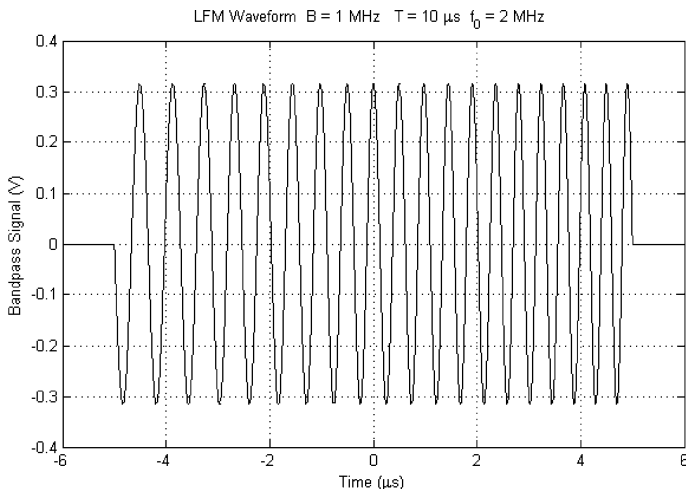


FIGURE 8.2 LFM bandpass signal example (shown for $T = 10 \mu\text{s}$, $B = 1 \text{ MHz}$, $f_0 = 2 \text{ MHz}$)

For the case of a large time-bandwidth, the magnitude of the autocorrelation function measured along the relative time delay axis is given by

$$|\chi_u(\tau, 0)| \approx |\text{sinc}(B\tau)|, |\tau| \ll T$$

The x -dB time delay resolution is measured between the values of τ for which

$$20\log|\text{sinc}(B\tau)| = -x \text{ (dB)}$$

The range resolution is equal to $c/2$ times the corresponding time delay resolution where c is the speed of light. Table 8.1 contains a summary of the resolution widths for the LFM waveform.

LFM Waveform Examples. Figure 8.3 shows the magnitude of the autocorrelation function as a function of relative time delay τ for doppler shifts[‡] of -0.5 MHz , 0 and 0.5 MHz , pulsedwidth $T = 10 \mu\text{s}$, swept bandwidth $B = 1 \text{ MHz}$, and LFM slope $\alpha = B/T = 0.1 \text{ MHz}/\mu\text{s}$. A doppler shift of $f_d = B/2 = 0.5 \text{ MHz}$ causes the peak of the correlation function to move to $\tau = f_d T/B = 5 \mu\text{s}$. Figure 8.4 shows the result when the pulsedwidth is increased to $100 \mu\text{s}$ to yield a waveform with an LFM slope equal

TABLE 8.1 LFM Waveform Time Delay and Range Resolution Widths

Mainlobe Width	Time Delay Resolution (s)	Range Resolution (m)
3.01 dB	$\tau_3 = 0.886/B$	$\Delta R_3 = 0.886c/B$
3.9 dB	$\tau_{3.9} = 1/B$	$\Delta R_{3.9} = c/2B$
6.02 dB	$\tau_6 = 1.206/B$	$\Delta R_6 = 1.206c/2B$
10.0 dB	$\tau_{10} = 1.476/B$	$\Delta R_{10} = 1.476c/2B$

[‡] These values of doppler shift are large for microwave radars and were selected to show the effect of range-doppler coupling.

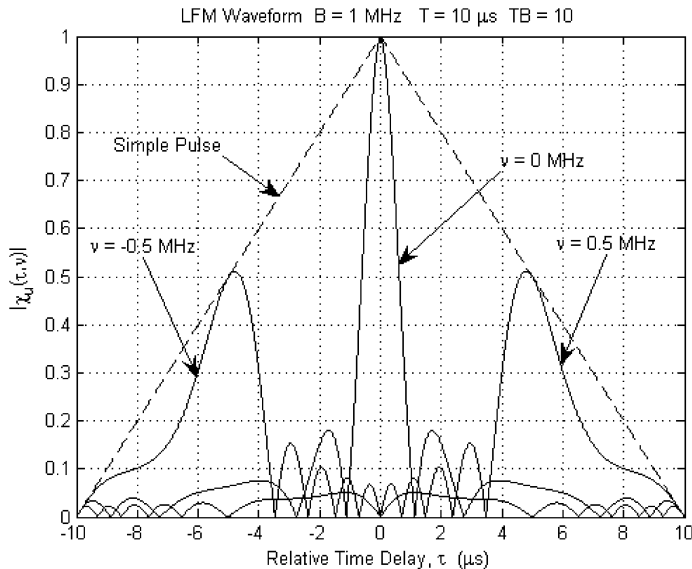


FIGURE 8.3 LFM waveform autocorrelation function ($T = 10 \mu\text{s}$, $B = 1 \text{ MHz}$, $TB = 10$)

to $0.01 \text{ MHz}/\mu\text{s}$. In this case, a doppler shift of 0.5 MHz shifts the peak of autocorrelation function to $\tau = 50 \mu\text{s}$, an increase of a factor of ten compared to the result for a $10-\mu\text{s}$ pulsewidth.

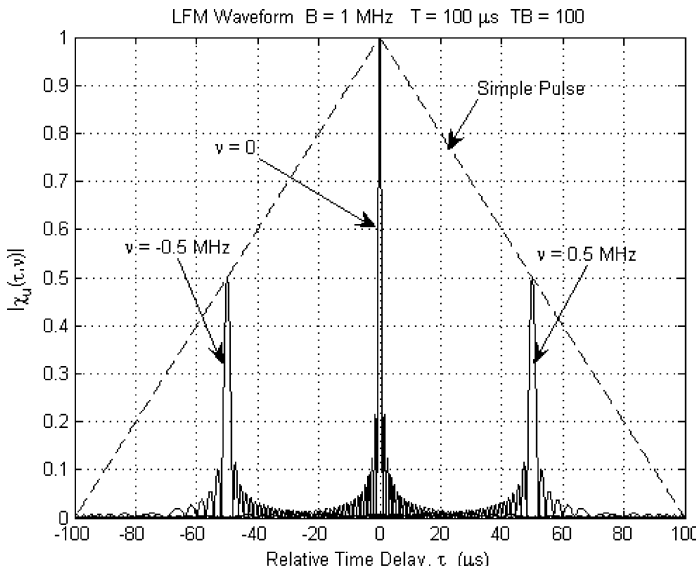


FIGURE 8.4 LFM waveform autocorrelation function ($T = 100 \mu\text{s}$, $B = 1 \text{ MHz}$, $TB = 100$)

Frequency Domain Weighting for LFM Time Sidelobe Reduction.^{1,2,4} A frequency domain weighting filter is used following the matched filter for time sidelobe reduction. Taylor weighting provides a realizable approximation to the ideal Dolph-Chebyshev weighting, which achieves the minimum mainlobe width for a given value of peak time sidelobe level. The frequency response of the equivalent low pass filter for the Taylor weighing filter is

$$W(f) = 1 + 2 \sum_{m=1}^{\bar{n}-1} F_m \cos\left(2\pi \frac{mf}{B}\right) \quad (8.10)$$

where F_m is the Taylor coefficient and \bar{n} is the number of terms in the weighting function. The compressed pulse response at the output of the weighting filter is given by

$$y_o(t) = \text{sinc}(Bt) + \sum_{m=1}^{\bar{n}-1} F_m [\text{sinc}(Bt+m) + \text{sinc}(Bt-m)] \quad (8.11)$$

As discussed below, the compressed pulse response (Eq. 8.11) is based on the assumption that the time-bandwidth product of the LFM waveform is much greater than unity ($TB \gg 1$). The filter matching loss for Taylor weighting is given by Klauder et al.¹ as

$$L_m = 1 + 2 \sum_{m=1}^{\bar{n}-1} F_m^2 \quad (8.12)$$

Figure 8.5 shows a comparison of the compressed pulse response for three frequency domain weighting types: Curve A is for uniform weighting where $W(f) = 1$

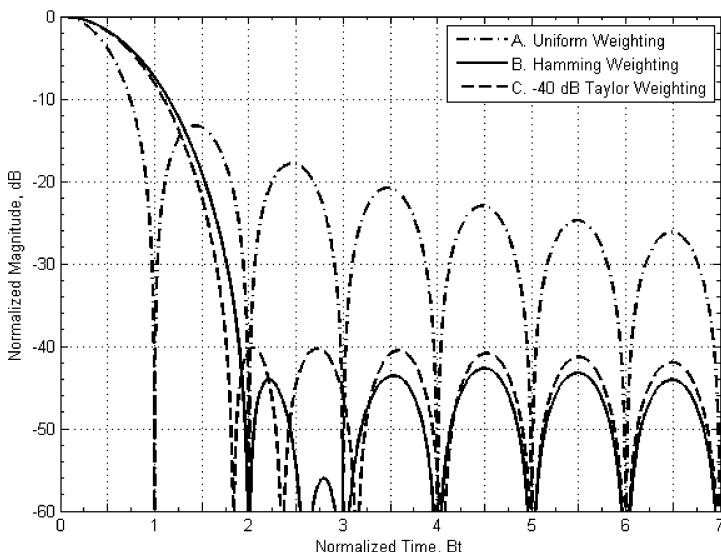


FIGURE 8.5 Comparison of compressed-pulse shapes for three frequency-domain weighting functions

(matched filter processing); Curve C is for Taylor weighting with -40 dB peak time sidelobe level ($\bar{n} = 6$); and Curve B is for Hamming weighting where

$$W(f) = 1 + 2F_1 \cos\left(2\pi \frac{mf}{B}\right)$$

$$F_1 = 0.4259 \quad (8.13)$$

The Taylor coefficients for -40 -dB Taylor weighting ($\bar{n} = 6$) are listed here:⁵

$$F_1 = 0.389116$$

$$F_2 = -0.00945245$$

$$F_3 = 0.00488172$$

$$F_4 = -0.00161019$$

$$F_5 = 0.000347037$$

Table 8.2 shows the peak time sidelobe level, 3-dB and 6-dB compressed-pulse widths, and filter matching loss for the three weighting function types. The application of -40 -dB Taylor weighting reduces the peak time sidelobe level from -13.2 dB to -40 dB and increases the filter matching loss from 0 dB to 1.15 dB. The 3-dB compressed-pulse mainlobe width increases from $0.886/B$ to $1.25/B$ when -40 -dB Taylor weighting is used. The 3-dB and 6-dB mainlobe widths and filter matching loss for Hamming weighting are approximately the same as for -40 -dB Taylor weighting.

These results assume that the time-bandwidth product of the LFM waveform is much greater than unity so that the time sidelobe performance is not limited by the Fresnel amplitude ripple in the spectrum of the LFM waveform. Cook and Paolillo³ and Cook and Bernfeld² have analyzed the effect of the Fresnel amplitude ripple and pulse rise-time and fall-time on time sidelobe levels. A phase predistortion technique is described by Cook and Paolillo,³ which reduces the Fresnel amplitude ripple to allow low time sidelobes to be achieved for LFM waveforms with relatively small time-bandwidth products.

Radar equipment distortion sources also establish limitations on achievable time sidelobe levels and are discussed by Klauder et al.¹ and Cook and Bernfeld.² The method of paired-echo analysis is used to evaluate the effect of amplitude and phase distortion on the time sidelobe levels. Frequency domain amplitude and phase distortion is typically caused by filters and transmission line reflections. Time domain amplitude and phase distortion, termed *modulation distortion* by Cook and Bernfeld, can result from power supply ripple in high-power transmitter amplifiers.²

TABLE 8.2 Comparison of LFM Weighting Filters

Weighting Function	Peak Time Sidelobe Level (dB)	3-dB Mainlobe Width, τ_3	6-dB Mainlobe Width, τ_3	Filter Matching Loss (dB)
Uniform	-13.2	$0.886/B$	$1.21/B$	0
Taylor (-40 dB, $\bar{n} = 6$)	-40	$1.25/B$	$1.73/B$	1.15
Hamming	-43	$1.30/B$	$1.81/B$	1.34

Taylor Versus Cosine-Squared-Plus-Pedestal Weighting. Figure 8.6a plots the taper coefficient F_1 and pedestal height H versus the peak time sidelobe level for cosine-squared-plus-pedestal weighting. For a given peak time sidelobe level, Taylor weighting offers theoretical advantages in range resolution and SNR performance, as illustrated in Figure 8.6b and Figure 8.6c.

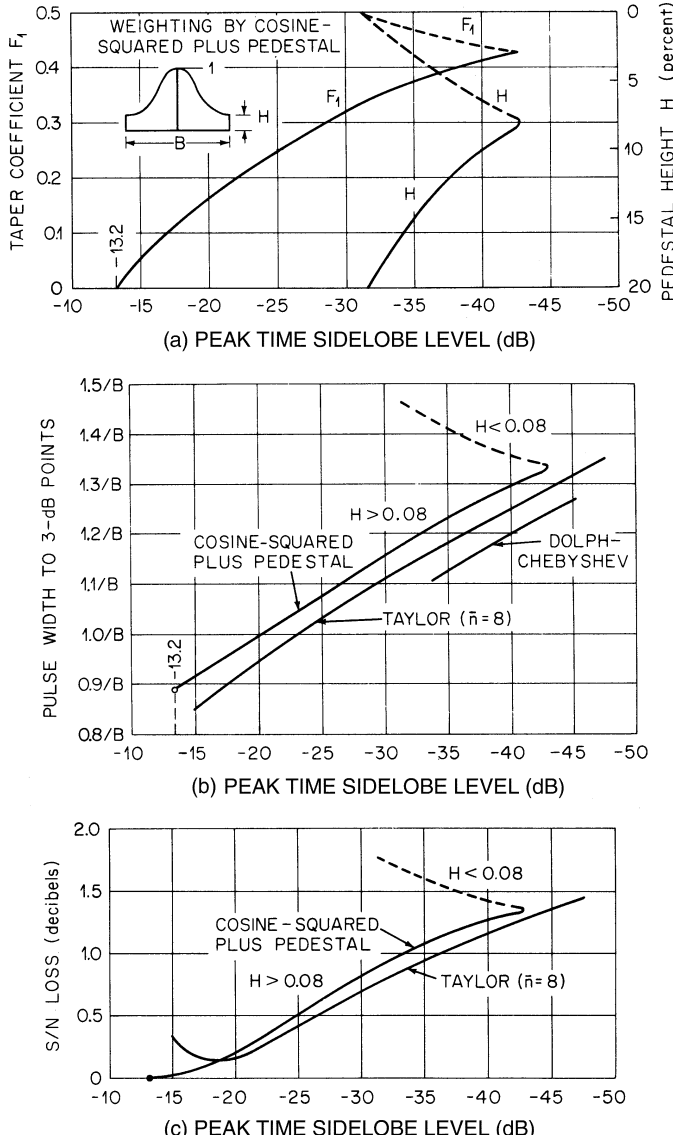


FIGURE 8.6 (a) Taper coefficient and pedestal height versus peak time sidelobe level; (b) Compressed-pulse width versus peak time sidelobe level; (c) SNR loss versus peak time sidelobe level

SAW Devices for LFM Pulse Compression. A Surface Acoustic Wave (SAW) device consists of an input transducer and an output transducer mounted on a piezoelectric substrate. These transducers are usually implemented as interdigital devices that consist of a metal film deposited on the surface of the acoustic medium. This metal film is made of fingers (see Figure 8.7) that dictate the frequency characteristic of the unit. The input transducer converts an electrical signal into a sound wave with over 95% of the energy traveling along the surface of the medium. The output transducer taps a portion of this surface sound wave and converts it back into an electric signal.

The SAW device⁶⁻⁸ has unique features that dictate its usefulness for a given radar application. It represents one of the few analog processing devices used in modern radar. The advantages of the SAW device are its compact size, the wide bandwidths that can be attained, the ability to tailor the transducers to a particular waveform, the all-range coverage of the device, and the low cost of reproducing a given design. The major shortcomings of the SAW approach are that the waveform length is restricted. Since sound travels about 3 to 15 mm/ μ s on the surface of a SAW device, a 250 mm quartz device (about the largest available), has a usable delay of about 70 μ s for a single pass.⁹ Also, because each SAW device is waveform specific, each waveform requires a different design.

SAW pulse compression devices depend on the interdigital transducer finger locations or the surface-etched grating to determine its bandpass characteristics. Figure 8.7 shows three types of filter determination approaches. A wideband input transducer and a frequency-selective (dispersive) output transducer are used in Figure 8.7a. When an impulse is applied to the input, the output signal is initially a low frequency that increases (based on the output transducer finger spacings) at later portions of the pulse. This results

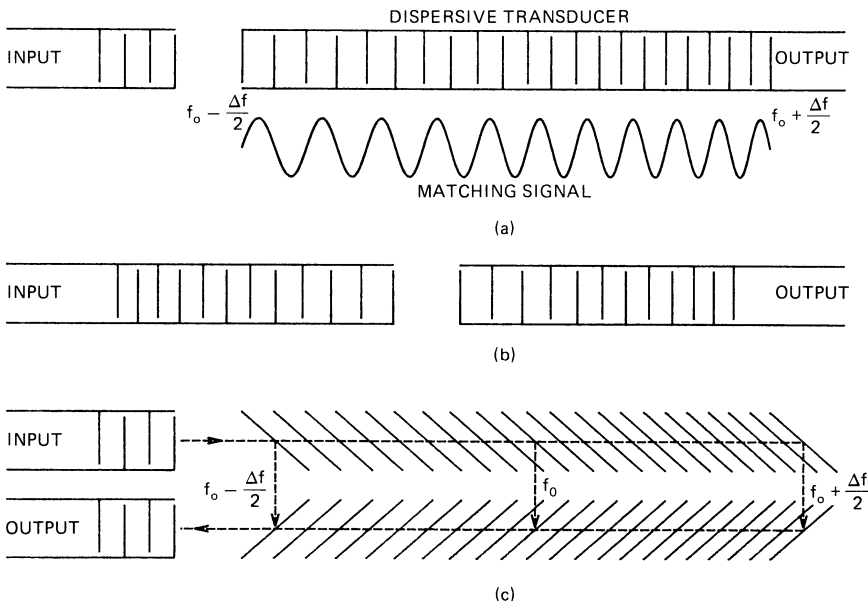


FIGURE 8.7 SAW transducer types: (a) dispersive output, (b) both input and output dispersive, and (c) dispersive reflections

in an up-chirp waveform that would be a matched filter for a down-chirp transmitted waveform. In Figure 8.7b both the input transducer and the output transducer are dispersive, which would result in the same impulse response as that shown in Figure 8.7a. For a given crystal length and material, the waveform duration for the approaches in Figure 8.7a and Figure 8.7b would be the same and is limited to the time that it takes an acoustic wave to traverse the crystal length. Figure 8.7c shows a reflection-array-compression (RAC) approach¹⁰ that essentially doubles the achievable pulse length for the same crystal length. In an RAC, the input and output transducers have a broad bandwidth. A frequency-sensitive grating is etched on the crystal surface to reflect a portion of the surface-wave signal to the output transducer. This grating coupling does not have a significant impact on the surface-wave energy. Except for a 2:1 increase in the waveform duration, the impulse response of the RAC is the same as for the approaches shown in Figure 8.7a and b. Thus, these three approaches yield a similar impulse response.

Figure 8.8 shows a sketch of a SAW pulse compression device with dispersive input and output transducers. As the energy in a SAW device is concentrated in its surface wave, the SAW approach is much more efficient than bulk-wave devices, where the wave travels through the crystal. The propagation velocity of the surface wave is in the range of 1500 to 4000 m/s, depending on the crystal material, and allows a large delay in a compact device. Acoustic absorber material is required at the crystal edges to reduce the reflections and, hence, the spurious responses. The upper frequency limit depends on the accuracy that can be achieved in the fabrication of the interdigital transducer. The SAW device must provide a response that is centered on a carrier, as the lowest frequency of operation is about 20 MHz and is limited by the crystal. A matched-filter SAW pulse compression device can use variable finger lengths to achieve frequency weighting, and this internal weighting can correct for the Fresnel amplitude ripples¹¹ in the FM spectrum. With this correction, -43 dB time sidelobe levels can be achieved for a linear-FM waveform with TB as low as 15. The level of sidelobe suppression depends upon the time bandwidth product, the weighting function applied, and fabrication errors in the SAW device. Time sidelobe levels of -35 dB have been achieved for TB between 5 and 15. TB products of up to 2000 have been achieved¹² with time sidelobes better than -40 dB.¹³ Dynamic range is limited by nonlinearities in the crystal material, but dynamic ranges over 90 dB have been achieved. The most common SAW materials are quartz, lithium niobate, and lithium tantalite.

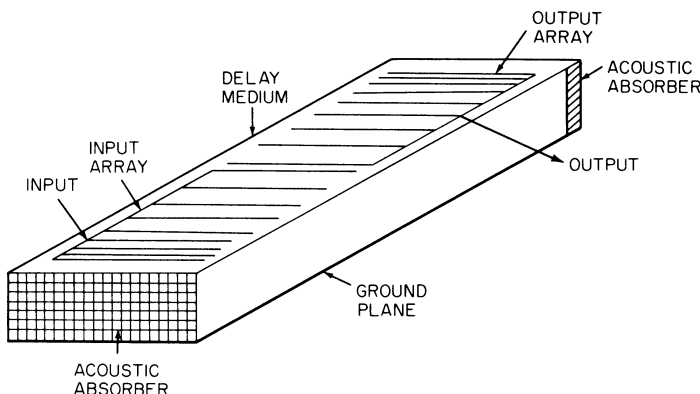


FIGURE 8.8 Surface-wave delay line

Nonlinear Frequency Modulation Waveforms. The nonlinear-FM waveform has several distinct advantages over LFM.^{14,16} It requires no frequency domain weighting for time sidelobe reduction because the FM modulation of the waveform is designed to provide the desired spectrum shape that yields the required time sidelobe level. This shaping is accomplished by increasing the rate of change of frequency modulation near the ends of the pulse and decreasing it near the center. This serves to taper the waveform spectrum so that the matched filter response has reduced time sidelobes.¹⁶ Thus, the loss in signal-to-noise ratio associated with frequency domain weighting (as for the LFM waveform) is eliminated.

If a symmetrical FM modulation is used (Figure 8.9a) with time-domain amplitude weighting to reduce the frequency sidelobes, the nonlinear-FM waveform will have a thumbtack-like ambiguity function (Figure 8.10). A symmetrical waveform typically has a frequency that increases (or decreases) with time during the first half of the pulse and decreases (or increases) during the last half of the pulse. A nonsymmetrical waveform is obtained by using one-half of a symmetrical waveform (Figure 8.9b). However, the nonsymmetrical waveform retains some of the range-doppler coupling of the linear-FM waveform.

One of the primary disadvantages of the nonlinear-FM waveform is that it is less doppler tolerant than the LFM. In the presence of doppler shift, the time sidelobes of the pulse-compressed NLFM tend to increase compared to those of the LFM. Figure 8.14, shown later in this section, and Table 8.3 illustrate this behavior for a typical NLFM pulse.

This characteristic of the NLFM waveform sometimes necessitates processing using multiple matched filters offset in doppler shift to achieve the required time sidelobe level. Because of the doppler sensitivity of the ambiguity function, the nonlinear frequency modulation waveform is useful in a tracking system where range and doppler frequency are approximately known, and the target doppler shift can be compensated in the matched filter. The nonsymmetrical NLFM waveform is used in the MMR system, for example, which detects and tracks ordnance such as mortars, artillery, and rockets.

To achieve a -40-dB Taylor compressed pulse response, for example, the frequency-versus-time (frequency modulation) function of a nonsymmetrical NLFM waveform of bandwidth B is¹⁴

$$f(t) = B \left(\frac{t}{T} + \sum_{n=1}^7 K_n \sin \frac{2\pi n t}{T} \right) \quad (8.14)$$

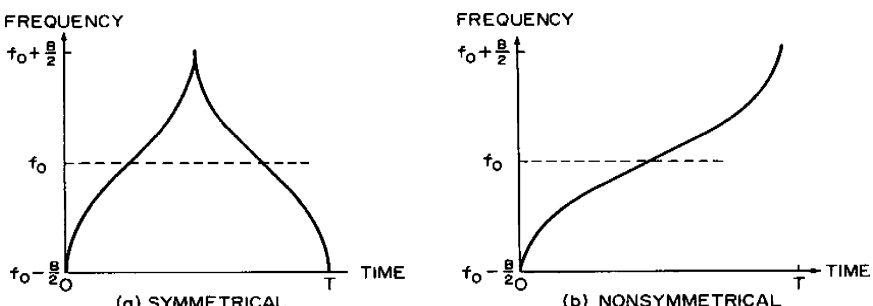


FIGURE 8.9 Symmetrical and nonsymmetrical nonlinear-FM waveforms

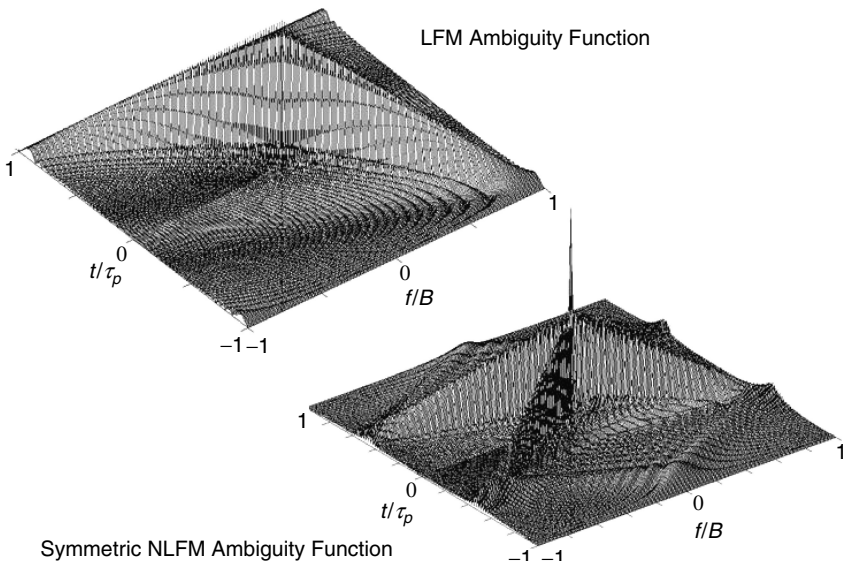


FIGURE 8.10 Ambiguity function of an LFM waveform compared to a symmetrical NLFM waveform

where the coefficients are

$$K_1 = -0.1145$$

$$K_2 = 0.0396$$

$$K_3 = -0.0202$$

$$K_4 = 0.0118$$

$$K_5 = 0.0082$$

$$K_6 = 0.0055$$

$$K_7 = -0.0040$$

Other NLFM waveforms that have been utilized in radar include the nonsymmetrical sine-based and tangent-based waveforms.[§] For the sine-based waveform, the relationship between time and frequency modulation is given as

$$\frac{t}{T} = \frac{f}{B} + \frac{k}{2\pi} \sin(2\pi f/B) \quad \text{for } -B/2 \leq f \leq B/2 \quad (8.15)$$

where T is the pulsewidth, B is the swept bandwidth, and k is a time sidelobe level control factor.

Typical k values are 0.64 and 0.70, which yield time sidelobe levels of -30 dB and -33 dB, respectively. Figure 8.11 is a plot of peak time sidelobe level as a function of the time sidelobe control factor k , for various TB products, for this NLFM waveform.

[§] Courtesy of Edwin M. Waterschoot, Lockheed Martin Maritime and Sensor Systems, Syracuse, NY.

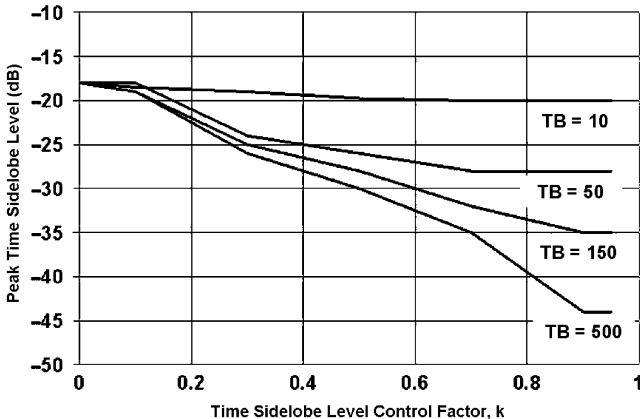


FIGURE 8.11 Peak time sidelobe level for a sine-based NLFM waveform as a function of k -factor (Courtesy of Dr. Peter H. Stockmann, Lockheed Martin Maritime and Sensor Systems, Syracuse, NY)

The frequency modulation-versus-time function for a tangent-based waveform is given as

$$f(t) = B \tan(2\beta t/T)/(2 \tan \beta) \quad \text{for } -T/2 \leq t \leq T/2 \quad (8.16)$$

where T is the pulsewidth, B is the swept bandwidth, and β is defined as

$$\beta = \tan^{-1}(\alpha), \quad 0 \leq \alpha < \infty$$

where α is a time sidelobe level control factor.

When α is zero, the tangent-based NLFM waveform reduces to an LFM waveform. However, α cannot be made arbitrarily large because the compressed pulse tends to distort. Collins and Atkins¹⁵ discuss an extension of the tangent-based NLFM for which the frequency modulation function is a weighted sum of tangent-based and linear frequency modulation terms.

Figure 8.12 shows the frequency modulation-versus-time functions for a sine-based NLFM waveform with $k = 0.6$, a tangent-based NLFM waveform with $\alpha = 2.5$, and an LFM waveform.

The sensitivity of a NLFM waveform to doppler shift can be seen in Figure 8.13, which shows the matched filter output for a sine-based NLFM waveform in the presence of doppler shift.

The ambiguity function of a NLFM sine-based waveform is shown in Figure 8.14. It can be noted that this ambiguity function is more thumbtack-like in nature than for an LFM waveform, indicating that this waveform is more doppler sensitive than the LFM waveform.

Table 8.3 provides a comparison of NLFM waveforms with weighted and unweighted LFM for different values of the target radial velocity in terms of peak and average time sidelobe levels and SNR loss. The NLFM waveform shows better

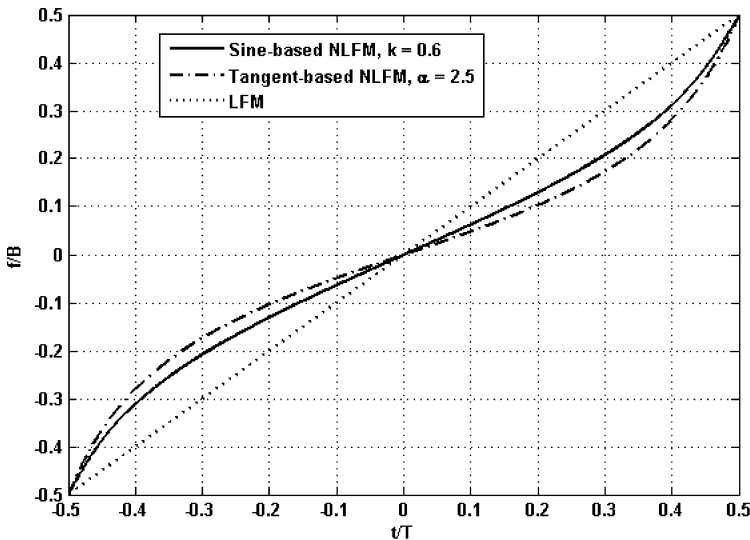


FIGURE 8.12 Frequency modulation-versus-time for sine-based NLFM, tangent-based NLFM, and LFM waveforms

performance in terms of SNR loss and peak time sidelobe level (TSL) than the LFM waveform. The TSL level does not degrade appreciably for the LFM waveform for higher radial velocities, demonstrating the higher doppler tolerance of LFM.

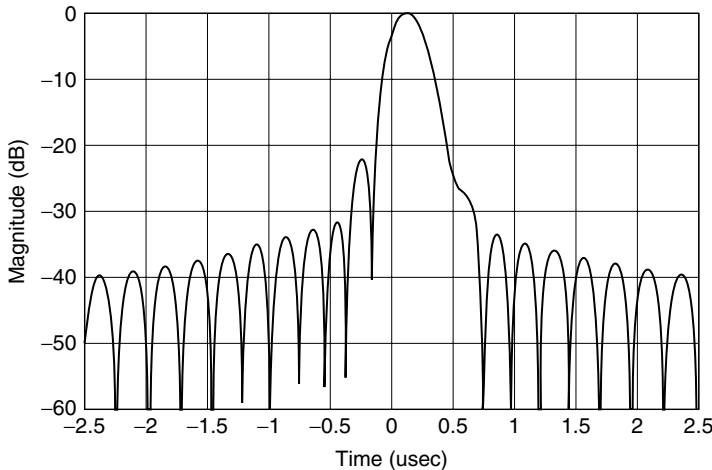


FIGURE 8.13 Matched filter output of S band, 44- μ s pulsewidth, 5-MHz bandwidth NLFM sine-based waveform with 500 m/s radial velocity (Courtesy of Edwin M. Waterschoot, Lockheed Martin Maritime and Sensor Systems, Syracuse, NY)

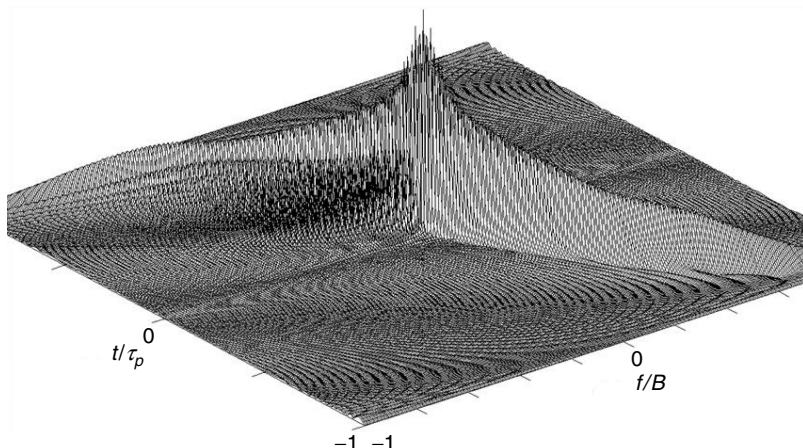


FIGURE 8.14 Ambiguity function of a sine-based symmetrical NLFM waveform

Phase-Coded Waveforms. In phase-coded waveforms, the pulse is subdivided into a number of subpulses each of duration $\delta = T/N$ where T is the pulsedwidth and N is the number of subpulses. Phase-coded waveforms are characterized by the phase modulation applied to each subpulse.

Binary Phase Codes. A phase-coded waveform that employs two phases is called *binary*, or *biphase*, coding. A binary phase-coded waveform is constant in magnitude with two phase values, 0° or 180° . The binary code consists of a sequence of either 0s and 1s or +1s and -1s. The phase of the signal alternates

TABLE 8.3 Comparison of Linear FM and Nonlinear FM Waveform Performance*

Weighting	Target Radial Velocity (m/s)*	Peak TSL (dB)	Average TSL (dB)**	Filter Matching Loss (dB)
LFM unweighted	0	-13.32	-36.59	0
LFM unweighted	± 300	-13.32	-36.56	0.024
LFM with -33 dB	0	-32.43	-49.27	0.843
Taylor weighting				
LFM with -33 dB	± 300	-32.25	-49.25	0.845
Taylor weighting				
Sine-based NLFM with $k = 0.70$	0	-32.67	-48.97	0
Sine-based NLFM with $k = 0.70$	± 300	-26.07	-47.99	0.038

* An S-band radar with 44-μs transmit pulsedwidth and 5-MHz bandwidth was used in this comparison.

The doppler shift expressed in Hz is $f_d = -(2/\lambda)V_r = -20V_r$ where V_r is the radial velocity expressed in m/s ($V_r > 0$ for an out-bound target).

** Average of TSL power ratio

between 0° and 180° in accordance with the sequence of elements, 0s and 1s or +1s and -1s, in the phase code, as shown in Figure 8.15. Because the frequency is not usually a multiple of the reciprocal of the subpulse width, the coded signal is generally discontinuous at the phase-reversal points. This does not impact its time sidelobes, but does cause some increase in the spectrum sidelobe levels.¹⁷

Upon reception, the compressed pulse is obtained by matched-filter processing. The width of the compressed pulse at the half-amplitude point is nominally equal to the subpulse width. The range resolution is hence proportional to the time duration of one element of the code (one subpulse). The time-bandwidth product and pulse compression ratio are equal to the number of subpulses in the waveform; i.e., the number of elements in the code.

Optimal Binary Codes. Optimal binary codes are binary sequences whose peak sidelobe of the aperiodic autocorrelation function is the minimum possible for a given code length. Codes whose autocorrelation function, or zero-doppler response, exhibit low sidelobes are desirable for pulse compression radars. Responses due to moving targets will differ from the zero-doppler response. If the matched filter is based only on the zero-doppler response, an increase in the time sidelobes will result. Ultimately, if the doppler shift becomes very large, the matched filter response will degrade. This can be alleviated by utilizing a bank of matched filters, covering the expected range of doppler shifts. Because this is more computationally intensive than a single matched filter, older radar systems tend not to employ banks of filters. The increase in computational capacity of modern radar systems, however, can make this more attractive.

Barker Codes. A special class of binary codes is the Barker¹⁸ codes. Barker codes are binary codes with peak time sidelobe levels equal to $-20\log(N)$, where N is the length of the code. The energy in the sidelobe region is minimum and uniformly distributed.¹⁹ The Barker code is the only uniform phase code that reaches this level.²⁰ All the known binary Barker codes are listed in Table 8.4. Only binary Barker codes of lengths 2, 3, 4, 5, 7, 11, and 13 have been found.²¹⁻²⁴

A pulse compression radar using Barker codes would be limited to a maximum time-bandwidth product of 13.²⁶ Figure 8.16 shows the autocorrelation function of

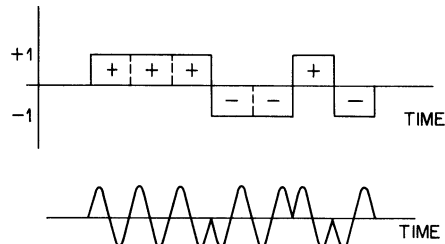


FIGURE 8.15 Binary phase-coded signal

TABLE 8.4 Known Binary Barker Codes²⁵

Length	Code
2	11, 10
3	110
4	1101, 1110
5	11101
7	1110010
11	11100010010
13	111100110101

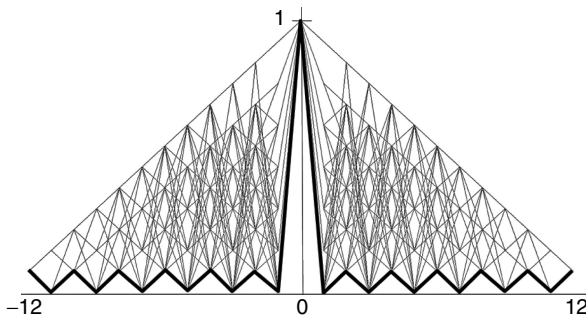


FIGURE 8.16 Superposition of the autocorrelation functions for all possible 13-bit code sequences with the Barker Code highlighted (dark), shown for zero doppler shift

a length 13 Barker code for zero doppler shift superimposed upon all possible autocorrelation functions of 13-bit binary sequences. It can be seen that the Barker code provides the lowest time sidelobe levels of all possible codes.

Allomorphic Forms. A binary code may be represented in any one of four allomorphic forms, all of which have the same correlation characteristics. These forms are the code itself, the inverted code (the code written in reverse order), the complemented code (1s changed to 0s and 0s to 1s), and the inverted complemented code. For symmetrical codes, the code and its inverse are identical.

Maximal-Length Sequences. Maximal-length sequences have a structure similar to random sequences and, therefore, possess desirable autocorrelation functions. They are often called *pseudorandom noise (PRN)* sequences. Historically, these sequences were generated using n stages of shift registers with selected output taps used for feedback (see Figure 8.17). When the feedback connections are properly chosen, the output is a sequence of maximal length, which is the maximum length of a sequence of 1s and 0s that can be formed before the sequence is repeated. The length of the maximal sequence is $N = 2^n - 1$, where n is the number of stages in the shift-register generator.

The feedback connections that provide the maximal-length sequences may be determined from a study of primitive and irreducible polynomials. An extensive list of these polynomials is given by Peterson and Weldon.²⁷

Although maximal-length sequences have some desirable autocorrelation characteristics, a maximum length sequence does not guarantee lowest time sidelobes when compared to other binary codes. An example of this is provided for a 15-bit sequence. Figure 8.18a is a histogram of the peak time sidelobe level for the autocorrelation of every possible combination of a 15-bit code. Figure 8.18b is the same but for only maximal length sequences of length 15 code (a subset of Figure 8.18a). Figure 8.18a shows a lowest time sidelobe level of -17.5 dB. The lowest sidelobe for the maximal length sequence is seen from Figure 8.18b to be only -14 dB.

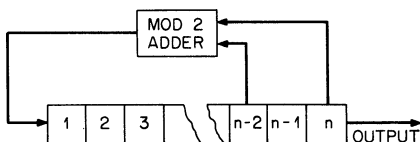


FIGURE 8.17 Shift-register generator

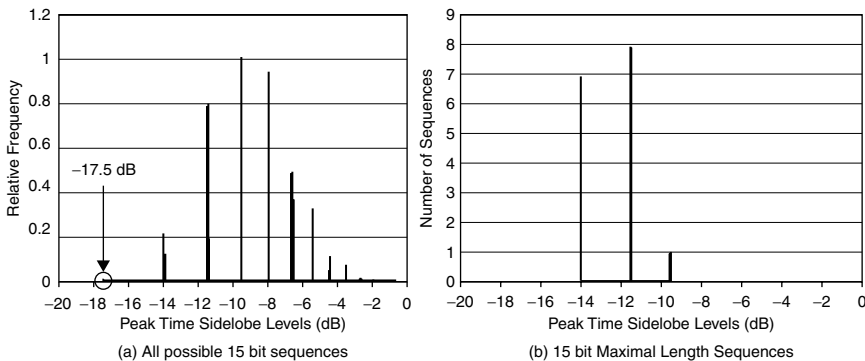


FIGURE 8.18 Histogram of peak time sidelobe levels for 15-bit sequences: (a) all possible 15-bit sequences and (b) 15-bit maximal length sequences

Minimum Peak Sidelobe Codes. Binary codes that provide minimum peak time sidelobe levels but exceed the time sidelobe levels achieved by Barker codes ($-20 \log(N)$) are termed minimum peak sidelobe codes.²⁹ These codes are usually found using computer search techniques. Skolnik²⁸ and Levanon and Mozeson²⁹ provide these codes for various sequence lengths, along with the resulting time sidelobe levels.

Complementary Sequences. Complementary sequences consist of two sequences of the same length N whose aperiodic autocorrelation functions have sidelobes equal in magnitude but opposite in sign. The sum of the two autocorrelation functions has a peak of $2N$ and a sidelobe level of 0. In a practical application, the two sequences must be separated in time, frequency, or polarization, which results in decorrelation of radar returns so that complete sidelobe cancellation may not occur. Hence, they have not been widely used in pulse compression radars.

Polyphase Codes. Waveforms consisting of more than two phases may also be used. Polyphase codes can be considered as complex sequences whose elements have a magnitude of one, but with variable phase.³⁰ The phases of the subpulses alternate among multiple values rather than just the 0° and 180° of binary phase codes. These codes tend to be discrete approximations to LFM waveforms, and hence possess similar ambiguity functions and doppler shift characteristics. The autocorrelation functions are similar, with a peak to sidelobe ratio of about \sqrt{N} .

Frank Codes. The Frank code corresponds to a stepped-phase approximation of an LFM waveform.³¹ Here, the pulse is broken up into M groups, each of which is further broken up into M subpulses. Hence, the total length of the Frank code, is M^2 , with a corresponding compression ratio of M^2 . The Frank polyphase codes³² derive the sequence of phases for the subpulses by using a matrix technique as follows:

$$\begin{bmatrix} 0 & 0 & 0 & \cdots & 0 \\ 0 & 1 & 2 & \cdots & (M-1) \\ 0 & 2 & 4 & \cdots & 2(M-1) \\ \vdots & \vdots & \vdots & \ddots & \vdots \\ 0 & (M-1) & 2(M-1) & \cdots & (M-1)^2 \end{bmatrix} \quad (8.17)$$

The matrix elements represent the multiplying coefficients of a basic phase shift $2\pi/M$, where M is an integer. The phase shift corresponding to the element m,n of the matrix can be written as

$$\phi_{m,n} = \frac{2\pi}{M}(m-1)(n-1), m = 1, \dots, M, n = 1, \dots, M \quad (8.18)$$

An example of a Frank Code matrix for $M = 4$ is given here:

$$\frac{\pi}{2} \begin{bmatrix} 0 & 0 & 0 & 0 \\ 0 & 1 & 2 & 3 \\ 0 & 2 & 4 & 6 \\ 0 & 3 & 6 & 9 \end{bmatrix} = \frac{\pi}{2} \begin{bmatrix} 0 & 0 & 0 & 0 \\ 0 & 1 & 2 & 3 \\ 0 & 2 & 0 & 2 \\ 0 & 3 & 2 & 1 \end{bmatrix} = \begin{bmatrix} 0 & 0 & 0 & 0 \\ 0 & 90^\circ & 180^\circ & 270^\circ \\ 0 & 180^\circ & 0 & 180^\circ \\ 0 & 270^\circ & 180^\circ & 90^\circ \end{bmatrix}$$

Concatenating the rows of this matrix yields the phase for each of the 16 subpulses. Figure 8.19 shows the phase modulation characteristic of the Frank Code for the above example. Note how the phase step between subpulses increases between subpulse groups with a length equal to four. This characteristic can be regarded as a stepped-phase approximation to quadratic phase modulation.

As M increases, the peak-sidelobe–voltage ratio approaches $(\pi M)^{-1}$. This corresponds to approximately a 10-dB improvement over pseudorandom sequences of similar length. The ambiguity function grossly resembles the knife-edge (ridge) characteristic associated with LFM waveforms, as contrasted with the thumbtack characteristic of pseudorandom sequences (Figure 8.20). However, for small ratios of doppler shift to waveform bandwidth, a good doppler response can be obtained for reasonable target velocities.

Lewis and Kretschmer Codes (P1, P2, P3, P4). Lewis and Kretschmer have studied the P1, P2, P3, and P4 polyphase codes.^{33,35} These codes are step approximations to the LFM pulse compression waveforms,³⁴ have low-range sidelobes, and have the

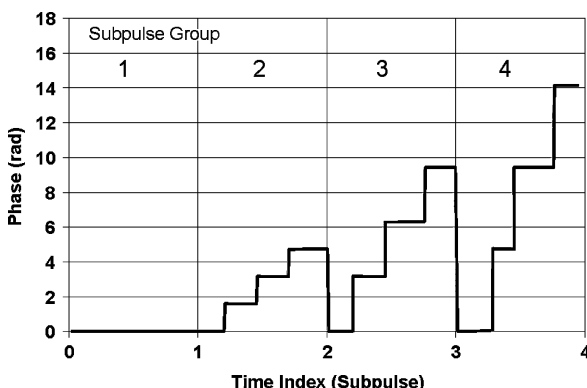


FIGURE 8.19 Phase versus time relationship for Frank code of length 16 ($M = 4$)

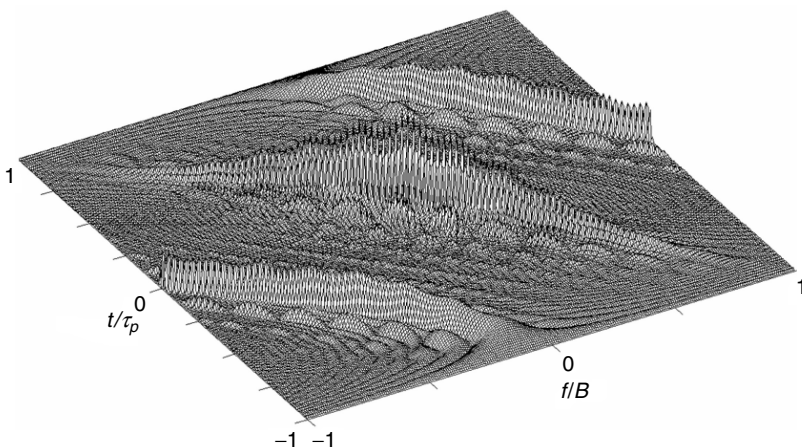


FIGURE 8.20 Ambiguity function of a Frank code of length 64 ($M = 8$)

doppler tolerance of the LFM codes. The P1 and P2 codes are modified versions of the Frank code with the DC frequency term at the center of the pulse instead of at the beginning. They are more tolerant of receiver band-limiting prior to pulse compression encountered in digital radar systems. The P1 codes contains M^2 elements as does the Frank code, but the relationship of the i th element to the j th group is expressed as³⁵

$$\phi_{i,j} = -(\pi/M)[M - (2j - 1)][(j - 1)M + (i - 1)] \quad (8.19)$$

where i and j are integers ranging from 1 to M .

P2 codes are similar, but the phase is symmetric with the following characteristic:

$$\phi_{i,j} = \{(\pi/2)[(M - 1)/M] - (\pi/M)(i - j)\}[M + 1 - 2j] \quad (8.20)$$

The P3 and P4 codes are derived by essentially converting an LFM waveform to baseband.³⁵ These tend to be more doppler tolerant than the Frank, P1, or P2 codes, and are also more tolerant of precompression bandwidth limitations that appear in radar systems. The phase of the P3 code is given as

$$\phi_n = \frac{\pi}{N} n^2 \quad n = 0, \dots, N - 1$$

The P4 code phase relationship is similar:

$$\phi_n = \frac{\pi n^2}{N} - \pi k \quad 0 \leq n \leq N$$

Table 8.5 summarizes the phase and autocorrelation characteristics of the Frank code and the Lewis and Kretschmer P1 through P4 polyphase codes.

TABLE 8.5 Summary of Phase and Autocorrelation Characteristics of Frank and Lewis and Kretschmer Polyphase Codes

Polyphase Code	Phase	Phase vs. Time Characteristic (N = 64 Example)	Autocorrelation (dB) (N = 64 Example)
Frank	$\frac{2\pi}{N}(i-1)(j-1)$ $i = 1, 2, 3, \dots, N$ $j = 1, 2, 3, \dots, N$		
P1	$-\frac{\pi}{M}[M - (2j-1)]$ $\bullet [(j-1)M + (i-1)]$ for ith element in the jth group		
P2	$\{(\pi/2)[(M-1)/M] - (\pi/M)(i-j)\}$ $\bullet [M+1-2j]$ for ith element in the jth group		
P3	$\frac{\pi}{N}n^2$ $n = 0, \dots, N-1$		
P4	$\frac{\pi n^2}{N} - \pi k$ $0 \leq n \leq N$		

P(n,k) Polyphase Codes. Whereas the previously discussed polyphase codes are derived from LFM waveforms, $P(n, k)$ codes are derived from step approximations of the phase characteristic of the weighting function of NLFM waveforms.²⁰ The weighting function is given by

$$W(f) = k + (1-k)\cos^n\left(\frac{\pi f}{B}\right) \quad (8.21)$$

where k and n are parameters of the weighting function, B is the swept bandwidth of the waveform, and $-B/2 \leq f \leq B/2$. This is a \cos^n weighting on a pedestal of height k (Figure 8.21). Hamming weighting is achieved for $n = 2$ and $k = 0.08$.

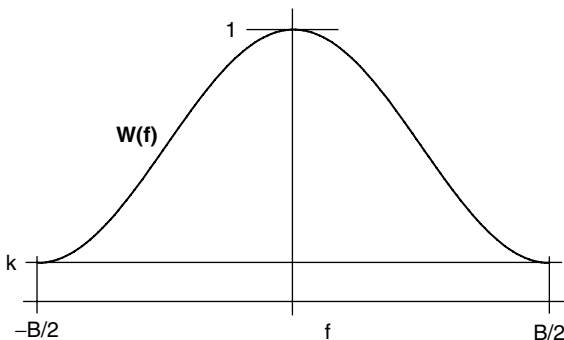


FIGURE 8.21 \cos^n on pedestal weighting function (shown for $n = 2$)

For the case where $n = 2$, the weighting function can be integrated to obtain the following relationship between time and frequency³¹

$$\frac{t}{T} = \frac{f}{B} + a \sin(2\pi f/B) \quad \text{where } a = (1 - k)/2(1 + k) \quad (8.22)$$

which is similar to the sine-based NLFM discussed earlier. This particular code is called Phase from Nonlinear Frequency (PNL)³¹ and its autocorrelation function is shown in Figure 8.22 for a 100- μ s pulsewidth, 1-MHz bandwidth waveform with $a = 0.7$ and $f_d = 0$. The time sidelobe levels are seen to be below -32 dB.

The ambiguity function is similar to that provided in the discussion of NLFM, which is expanded in Figure 8.23 to show in more detail the impact of doppler shift on the pulse compressed waveform for practical values of doppler shifts.

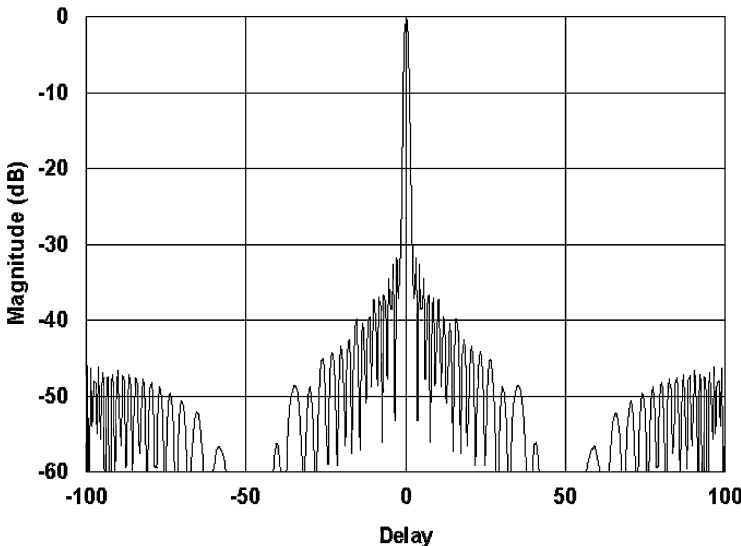


FIGURE 8.22 100- μ s PNL pulse autocorrelation function for $TB = 100$, $a = 0.7$, and $f_d = 0$

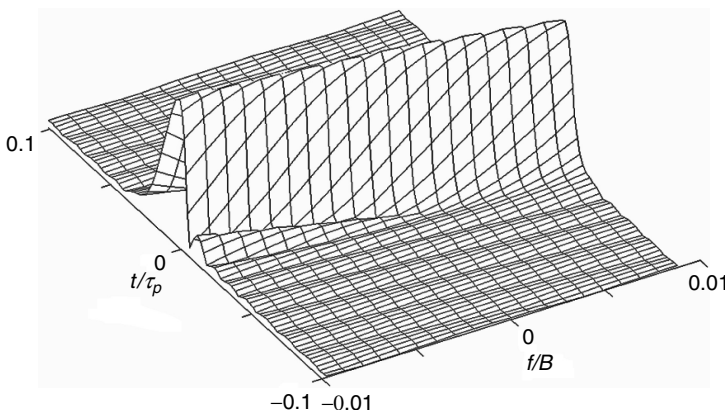


FIGURE 8.23 Expanded view of PNL ambiguity diagram for 100- μ s pulse, $a = 0.7$, and $B = 1$ MHz

As the doppler shift moves away from zero, the peak decreases and the close-in time sidelobe levels on one side or the other begin to increase. Note that an f/B ratio of 0.01 corresponds to a doppler shift associated with approximately a Mach 1 target at a S band carrier frequency.

In general for $P(n, k)$ waveforms, the integral of the weighting function provides the relationship between time and frequency modulation as shown in Eq. 8.23:

$$\frac{t}{T} = \frac{1}{\pi} \int_{-\frac{\pi}{2}}^{\frac{\pi f}{B}} [k + (1-k)\cos^n(x)] dx \quad (8.23)$$

Since frequency modulation is proportional to the time derivative of phase, phase is obtained by integrating the frequency with respect to time. The expression for frequency, however, is not straightforward, and is usually obtained through numerical evaluation.³¹

Quadriphase Codes. Quadriphase codes are an example of a phase-coded waveform without phase discontinuities. Quadriphase codes^{36,37} are based on the use of subpulses with a half-cosine shape and phase changes between adjacent subpulses of multiples of $\pm 90^\circ$. The cosine weighting provides faster spectrum roll-off, lower filter matching loss, and smaller range sampling loss when compared to rectangular subpulse phase-coded waveforms (Table 8.6).

TABLE 8.6 Quadriphase Waveform Performance Summary³⁶

	Quadriphase Code	Rectangular Subpulse Code
Radiated Spectrum 40-dB Width	$5/\delta$	$64/\delta$
Falloff (δ = subpulse duration)	12 dB/Octave	6 dB/Octave
Range Sampling Loss	0.8 dB	2.3 dB
Filter Matching Loss	0.1 dB	0.5 dB

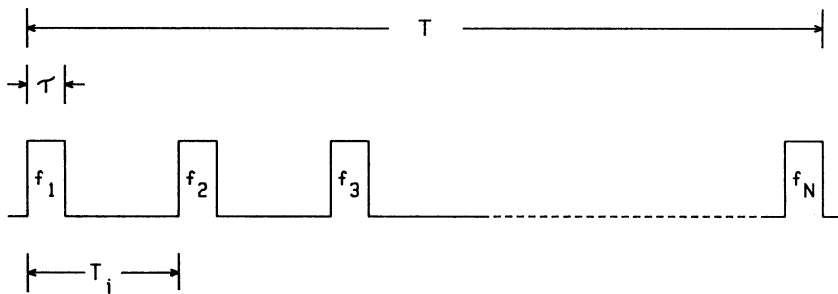


FIGURE 8.24 Time-frequency-coded waveform

Time-Frequency-Coded Waveforms. A time-frequency-coded waveform (Figure 8.24) consists of a train of N pulses with each pulse at a different frequency.³⁸ Generally, the frequencies are equally spaced, and the pulses are of the same amplitude. The ambiguity function for a periodic waveform of this type consists of a central spike plus multiple spikes or ridges displaced in time and frequency. Although it is unachievable in practice, the objective is to create a high-resolution, thumbtack-like central spike with a clear area around it. Measurement is then performed on the high-resolution central spike. The range resolution or compressed-pulse width is determined by the total bandwidth of all the pulses, and the doppler resolution is determined by the reciprocal of the waveform duration T . For example, a typical waveform in this class has N contiguous pulses of width τ whose spectra of width $1/\tau$ are placed side by side in frequency to eliminate gaps in the composite spectrum. Since the waveform bandwidth is now N/τ , the nominal compressed-pulse width is τ/N . These relationships are summarized in Table 8.7.

Shaping of the high-resolution central spike area as well as the gross structure of the ambiguity surface can be accomplished by variations of the basic waveform parameters, such as amplitude weighting of the pulse train, staggering of the pulse repetition interval, and frequency or phase coding of the individual pulses.³⁹

Costas Codes. Costas codes are a class of frequency-coded waveforms that have near ideal range and doppler sidelobe behavior.^{40,41} In other words, their ambiguity function approaches the ideal thumbtack, providing both doppler and range information (Figure 8.25). All sidelobes, except for a few near the origin, have an amplitude of $1/M$. A few sidelobes close to the origin are about twice as large, or about $2/M$, which is characteristic of Costas codes. The compression ratio of a Costas code is about $M^{1/2}$.

The Costas code is a burst of M contiguous uncoded pulse waveforms, each with a different frequency selected from a finite set of M equally spaced frequencies⁴³ that are

TABLE 8.7 N Pulses Contiguous in Time and Frequency

Waveform duration, T	$N\tau$
Waveform bandwidth, B	N/τ
Time-bandwidth product, TB	N^2
Compressed pulse width, $1/B$	$\tau/N = \tau/N^2$
Doppler resolution, $1/T$	$1/N\tau$

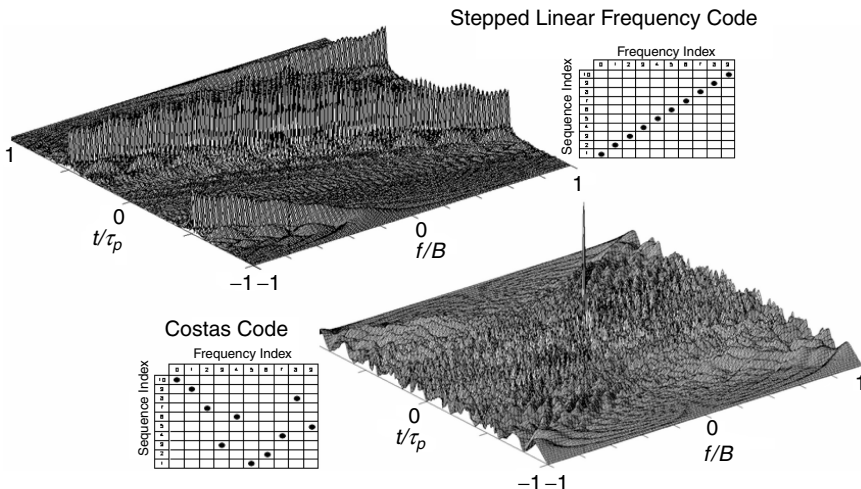


FIGURE 8.25 Comparison of ambiguity functions for $N = 10$ stepped linear and Costas sequence showing the impact of frequency order⁴⁰

processed coherently. The order in which the frequencies are generated greatly influences the nature of the ambiguity function of the burst. If the frequencies are monotonically increasing or decreasing, the waveform is simply a stepped approximation to an LFM, which has a ridge in its ambiguity function (Figure 8.25). In order to approach a thumbtack-like ambiguity function, the order of the frequencies needs to be more random in nature. The order of frequencies is the code, and it is generated via a special class of $M \times M$ Costas arrays. Costas^{41,44} suggested a technique for selecting the order of these frequencies to provide more controlled range and doppler sidelobes. An example of a Costas code of length 10 is shown in Figure 8.25, as it compares to the stepped LFM. Tables showing the sequence order for each waveform are also provided.

8.3 FACTORS AFFECTING CHOICE OF PULSE COMPRESSION SYSTEMS

The choice of a pulse compression system involves the selection of the type of waveform and the method of generation and processing. Methods of generating and processing pulse compression waveforms are discussed in the section on pulse compression implementation in this chapter. Discussions here will concentrate on the waveform itself. The primary factors influencing the selection of a particular waveform are usually the radar requirements of doppler tolerance and time sidelobe levels.

Table 8.8 summarizes these factors for three FM types: LFM, NLFM, and phase-coded waveforms. The systems are compared on the assumption that information is extracted by processing a single waveform as opposed to multiple-pulse processing. The symbols B and T denote the bandwidth and the pulselength of the waveform, respectively.

In cases where an insufficient doppler shift occurs, such as with a stationary or tangential target, range resolution is the chief means for seeing a target in clutter.

TABLE 8.8 Comparisons of Performance Characteristics for LFM, NLFM, and Phase-Coded Waveforms

Factor	Linear FM	Nonlinear FM	Binary Phase Coded	Polyphase Coded
Doppler tolerance	Supports doppler shifts up to $\pm B/10$. Time shift of $f_d T/B$ is introduced by range-doppler coupling. Time sidelobe performance remains excellent for large doppler shifts.	Adequate insensitivity to doppler to allow use generally up to Mach 1. Time shift of $f_d T/B$ is introduced by range-doppler coupling for a nonsymmetrical NLFM waveform. Common, therefore, in ATC radars. Multiple tuned pulse compressors required for high-speed targets.	Higher sensitivity to doppler shift. Time sidelobes increase while mainlobe response decreases for higher doppler (characteristic of a thumbtack-like ambiguity function). Used, therefore, for low-speed target applications and with small TB products.	Highest sensitivity to doppler shift. Time sidelobes increase while mainlobe response decreases for higher doppler (characteristic of a thumbtack-like ambiguity function). Used, therefore, for low-speed target applications and with small TB products. Longer phase-coded waveforms are more sensitive to doppler shifts than the shorter ones.
Time sidelobe level	Adequate weighting, high TB product, and low amplitude and phase errors are necessary to achieve good time sidelobes.	For nonsymmetrical NLFM, excellent time sidelobes if there is adequate NLFM phase coding, a high TB product, and sufficiently low amplitude and phase errors. Increasing NLFM phase code weighting introduces increased radial velocity sensitivity.	Good time sidelobes that are determined by coding.	Better time sidelobes than binary phase-coded waveforms.
General	Often used for high-speed target capability ($> M$ ach 1). Extremely wide bandwidths achievable.	Use is generally restricted to applications where primary target radial velocities $< M$ ach 1. Multiple tuned matched filters are generally not computationally practical.	Generally found in low doppler shift applications.	Generally found in low doppler shift applications.

Clutter rejection with pulse compression waveforms is due to the greater range resolution achievable over uncoded waveforms. Because the range resolution is proportional to the reciprocal of the bandwidth, wider-bandwidth pulse compression waveforms can offer greater clutter rejection.

8.4 PULSE COMPRESSION IMPLEMENTATION AND RADAR SYSTEM EXAMPLES

This section describes the generation and processing of pulse compression waveforms and provides examples of radar systems that utilize these processing techniques. Major advances are continually being made in the devices and techniques used in pulse compression radars. Significant advances are evident in the digital and SAW techniques that allow the implementation of a variety of pulse compression waveform types. The digital approach has blossomed because of the manifold increase in computational speed and also because of the size reduction and the speed increase of the memory units. SAW technology has expanded because of the invention of the interdigital transducer,⁴⁵ which provides efficient transformation of an electrical signal into acoustic energy and vice versa.

Digital Waveform Generation. Figure 8.26 shows a digital approach⁴⁶ for generating the radar waveform. The phase control element supplies digital samples of the in-phase component I and the quadrature component Q , which are converted to their analog equivalents. These phase samples may define the baseband components of the desired waveform, or they may define the waveform components on a low-frequency carrier. If the waveform is on a carrier, the balanced modulator is not required, and the filtered components would be added directly. The sample-and-hold circuit removes the transients due to the nonzero transition time of the digital-to-analog (D/A) converter. The low-pass filter smoothes (or interpolates) the analog signal components between waveform samples to provide the equivalent of a much higher waveform-sampling rate. The $I(t)$ component modulates a 0° carrier signal, and the $Q(t)$ component modulates a 90° phase-shifted carrier signal. The desired waveform is the sum of the 0° -modulated carrier and the 90° -modulated carrier. As mentioned earlier, when the digital phase samples include the carrier components, the I and Q components are centered on this carrier frequency and the low-pass filter can be replaced with a bandpass filter centered on the IF carrier.

When a linear-FM waveform is desired, the phase samples follow a quadratic pattern and can be generated by two cascaded digital integrators. The input digital command to the first integrator defines this quadratic phase function. The digital command to the second integrator is the output of the first integrator plus the desired carrier frequency. This carrier may be defined by the initial value of the first integrator. The desired initial phase of the waveform is the initial value of the second integrator or else may be added to the second-integrator output.

With advances in digital technology, it has become possible and practical to generate waveforms directly at IF or RF carrier frequencies on a single integrated circuit chip. This technique is called *Direct Digital Synthesis*, or DDS, and involves generating waveforms at

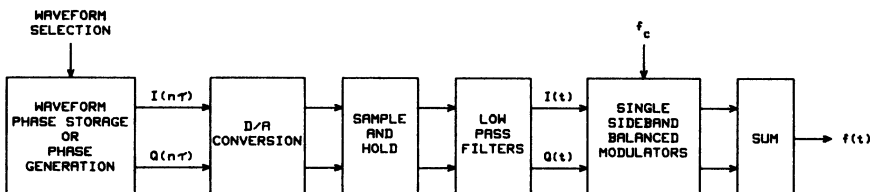


FIGURE 8.26 Digital waveform generation block diagram

high sampling rates and filtering the output. These devices generate the waveform by accumulating phase information, which is then used to look up values of the waveform (usually a sine wave). This is converted to an analog signal with a digital-to-analog converter (DAC or D/A converter) and filtered. A variety of waveform types (e.g., LFM, NLFM, and CW waveforms) can be generated in this way by using the appropriate phase modulation characteristic. As an example, the Analog Devices AD9858 Direct Digital Synthesizer⁴⁷ uses a 10-bit DAC operating at up to a 1-GHz internal clock speed (DAC update rate).

Digital Pulse Compression.^{48–50} Digital pulse compression techniques are routinely used for matched filtering of radar waveforms. The matched filter may be implemented by using a digital convolution for any waveform or else by use of stretch processing for a linear-FM waveform.

Digital pulse compression has distinct features that determine its acceptability for a particular radar application. Digital matched filtering usually requires multiple overlapped processing units for extended range coverage. The advantages of the digital approach are that long-duration waveforms present no problem, the results are extremely stable under a wide variety of operating conditions, and the same implementation could be used to handle multiple waveform types.

Analog product detectors used to extract *I* and *Q* baseband components have been replaced in many systems by digital down-conversion techniques. In this approach, the complex envelope sequence is evaluated by digital signal processing of A/D converter samples at the final IF output of the receiver, rather than by separate A/D conversion of baseband analog *I* and *Q* components.^{51–53} Digital down-conversion is advantageous because performance is not limited by amplitude and phase imbalances that exist in analog product-detection hardware.

Figure 8.27 illustrates two digital signal-processing approaches to providing the matched filter for a pulse compression waveform. In both cases, the input signal is the complex envelope sequence as formed using either digital down-conversion or analog

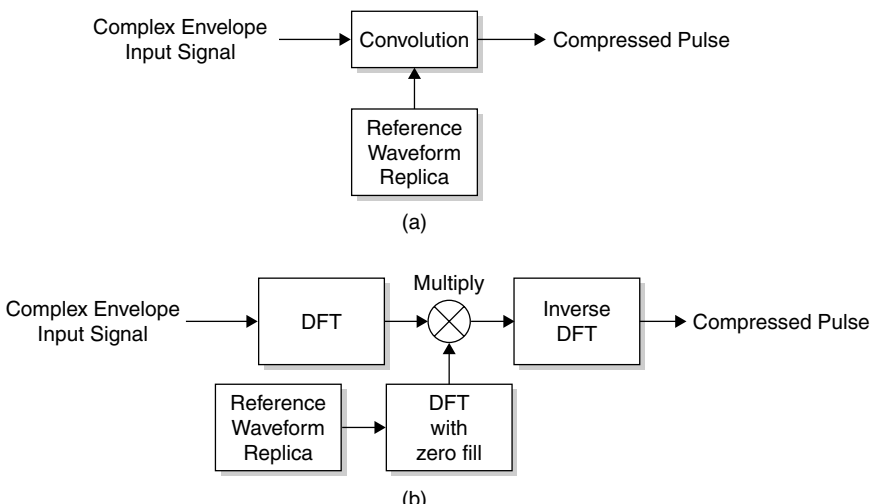


FIGURE 8.27 (a) Time-domain digital pulse compression processor and (b) frequency-domain digital pulse compression processor

product detection followed by A/D conversion in each baseband channel. Figure 8.27a shows a digital implementation of a time-domain convolution processor that will provide matched-filter performance for any radar waveform. In this case, discrete-time convolution is done in the time domain by convolution of the complex envelope input sequence following digital down-conversion with the matched filter impulse response sequence. Because time-domain convolution can be computationally intensive, a more economical approach from a computational standpoint is shown in Figure 8.27b, in which frequency-domain processing is used to implement the convolution.

The frequency-domain digital pulse compression processor operates on the principle that the discrete Fourier transform (DFT) of the time convolution of two sequences is equal to the product of the discrete Fourier transforms of each of the sequences. If M range samples are to be provided by one processor, the length of the DFT must exceed M plus the number of samples in the reference waveform minus one to achieve an aperiodic convolution. These added M samples are filled with zeros in the reference waveform DFT. For extended range coverage, repeated processing operations are required with range delays of M samples between adjacent operations using the overlap-save convolution technique.^{49,54} This processor can be used with any waveform, and the reference waveform can be offset in doppler frequency to achieve a matched filter at this doppler frequency.

Pulse Compression Radar Examples. There are many radars under development or deployed that utilize some of the pulse compression waveforms previously discussed. Advances in digital signal-processing technology have enabled a wider variety of waveform implementations. For example, radar systems are no longer limited to the LFM waveform; instead, radar system capabilities can be extended to take advantage of the more complex processing associated with the nonlinear FM waveform.

*AN/TPS-59 and AN/FPS-117 Surveillance Radars.*⁵⁵ The AN/TPS-59 and AN/FPS-117 are a family of L band, long-range surveillance radars that employ LFM waveforms. The antenna is mechanically rotated in azimuth, and electronic pencil-beam scanning is performed in elevation. The transmission utilizes two time-sequenced LFM pulses of different frequencies in order to create Swerling Case 2 target statistics. Both radars employ frequency-domain digital pulse compression processing.

Air Surveillance and Precision Approach Radar System. The Air Surveillance and Precision Approach Radar System (ASPARCS) is intended to provide the next-generation air traffic control (ATC) radar, as part of the Multi-Mission Surveillance Radar (MMSR) family of ATC radars built by Lockheed Martin Co. Nonlinear FM waveforms are used because the targets of interest have relatively low doppler shifts (less than Mach 1). Like the AN/FPS-117 radar, this system implements frequency-domain digital pulse compression processing.

Multi-Mission Radar. The Multi-Mission Radar (MMR) is designed to detect and track mortars, artillery, and rockets. This radar uses a nonlinear FM sine-based waveform. Digital frequency-domain pulse compression processing is performed.

*ASR-12 Next-Generation Solid-State Air Traffic Control Radar.*⁵⁶ The ASR-12 terminal airport surveillance radar transmits a 55- μ s pulse with peak power of 21 kW to provide a single-pulse transmit energy of 1.16 J. Nonlinear frequency modulation is used with a pulse compression ratio of 55 to achieve range-resolution equivalent to an uncoded 1- μ s pulse. The filter matching loss is less than 0.6 dB and typical time

sidelobe levels measured on production hardware are -58 dB. Digital pulse compression is used. An uncoded $1.1\text{-}\mu\text{s}$ pulse is used to provide coverage for targets within the range interval from 0.5 to 5.5 nmi.

Stretch Pulse Compression.^{57–60,62} Stretch pulse compression is a technique for performing LFM pulse compression of wideband waveforms using a signal processor with bandwidth that is much smaller than the waveform bandwidth, without loss of signal-to-noise ratio or range resolution. Stretch pulse compression is used for a single target or for multiple targets that are located within a relatively small range window centered at a selected range.

Figure 8.28 shows a block diagram of a stretch pulse compression system. The LFM waveform has a swept bandwidth B , pulselength T , and LFM slope α . The reference waveform is generated with time delay τ_R , swept bandwidth B_R , pulselength T_R , and LFM slope α_R . The reference waveform time delay is typically derived by range tracking of a selected target within the range window. The correlation mixer^{62,63} (CM) in Figure 8.29 performs a bandpass multiplication of the received signal by the output of the reference waveform generator. The lower sideband at the CM output is selected by a bandpass filter (BPF).

Spectrum analysis is performed when the LFM slopes of the transmit and reference waveforms are equal ($\alpha = \alpha_R$). Reduced-bandwidth pulse compression processing is performed if the reference waveform LFM slope is less than the transmit waveform LFM slope ($\alpha_R < \alpha$). In both cases, the required processing bandwidth B_p is much smaller than the waveform bandwidth.

Figure 8.29 shows the principle of stretch pulse compression for the case where the LFM slopes of the transmit and reference waveforms are equal. The instantaneous frequency is plotted as a function of time at three points in the stretch pulse compression system block diagram: (1) correlation mixer input, (2) correlation mixer LO (reference waveform generator output), and (3) correlation mixer output (output of bandpass filter). Three LFM target signals are shown at the correlation mixer input: target 1 is at zero time offset relative to the reference waveform; target 2 is earlier in time than the reference waveform; and target 3 is later in time. In each case, the LFM slope for the target signals is B/T . The reference waveform applied to the LO port of the CM has LFM slope equal to $B_R/T_R = B/T$.

The instantaneous frequency at the correlation mixer output is the difference between the instantaneous frequencies at the CM input and LO ports. As a result, the CM output signals for the three target signals are uncoded pulses (pulsed CW signals) with frequency offset from the mixer IF output f_{IF} given by

$$\delta f = -\left(\frac{B}{T}\right)t_d \quad (8.24)$$

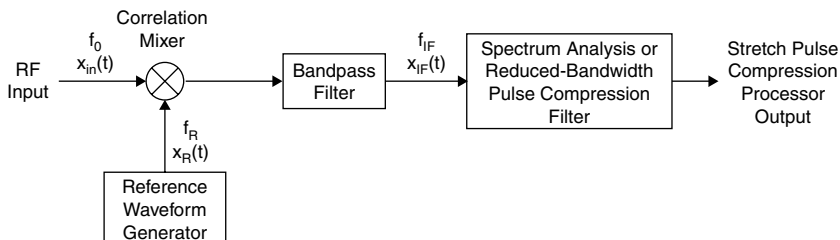


FIGURE 8.28 Stretch pulse compression system block diagram

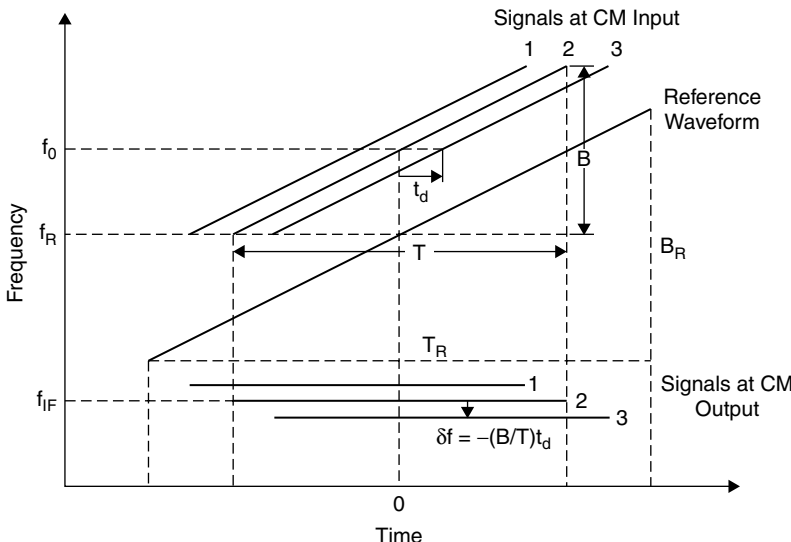


FIGURE 8.29 Correlation mixer signals in stretch pulse compression (after Roth et al.⁶¹)

where t_d is the time delay of the midpoint of the signal measured relative to the midpoint of the reference waveform. For the case shown, where the RF carrier frequency is above the carrier frequency of the reference waveform, a positive time delay results in a negative frequency offset. The signals at the correlation mixer output are then resolved in the frequency domain by spectral analysis processing.

A typical implementation for the spectral analysis processing includes a second frequency conversion following the CM to a final intermediate frequency (IF), anti-aliasing filtering, direct sampling at the final IF using an analog-to-digital converter (ADC), digital down conversion (DDC) to a complex envelope sequence, time-domain weighting, and spectral analysis using an FFT padded with zeros.⁶⁴ Previous implementations used analog product detectors to extract I and Q baseband signals, with separate ADCs in the I and Q baseband channels.

Correlation Mixer Output Signal Analysis. The received signal at the CM input port from a point target is

$$x_{in}(t) = A \operatorname{rect}\left(\frac{t-\tau}{T}\right) \cos[2\pi(f_0 + f_d)(t-\tau) + \pi\alpha(t-\tau)^2] \quad (8.25)$$

where A is the amplitude, T is the transmit pulselength, f_0 is the carrier frequency, f_d is the doppler frequency, τ is the signal time delay, and α is the LFM slope for the transmit waveform. The reference waveform applied to the LO port is

$$x_R(t) = 2 \operatorname{rect}\left(\frac{t-\tau_R}{T_R}\right) \cos[2\pi f_R(t-\tau_R) + \pi\alpha_R(t-\tau_R)^2] \quad (8.26)$$

where T_R is the pulselength, f_R is the carrier frequency, τ_R is the reference waveform time delay, and α_R is the LFM slope for the reference waveform ($\alpha_R \leq \alpha$).

The correlation mixer acts as a bandpass multiplier with output $x_{\text{in}}(t)x_R(t)$. The IF output of the correlation mixer is evaluated using the identity

$$2\cos x \cos y = \cos(x + y) + \cos(x - y)$$

where the first term on the right-hand side of the equation corresponds to the upper sideband and the second to the lower sideband at the mixer output. The upper sideband is rejected by the bandpass filter to yield

$$\begin{aligned} x_{\text{IF}}(t) &= A \operatorname{rect}\left(\frac{t - \tau}{T}\right) \operatorname{rect}\left(\frac{t - \tau_R}{T_R}\right) \\ &\cdot \cos[2\pi f_{\text{IF}}(t - \tau) + 2\pi f_d(t - \tau) + 2\pi\alpha_R(\tau_R - \tau)(t - \tau) + \pi(\alpha - \alpha_R)(t - \tau)^2 + \phi] \end{aligned} \quad (8.27)$$

where $f_{\text{IF}} = f_0 - f_R$ is the IF carrier frequency ($f_0 > f_R$ is assumed) and the carrier phase shift is

$$\phi = -2\pi f_R(\tau - \tau_R) - 2\pi\alpha_R(\tau - \tau_R)^2$$

The IF signal is an LFM waveform with reduced slope $\alpha - \alpha_R$ (the factor that multiplies the quadratic term in the argument of the cosine) and a frequency offset relative to the IF carrier frequency f_{IF} given by

$$\delta f = f_d + \alpha_R(\tau_R - \tau) \quad (8.28)$$

The duration of the reference waveform is required to exceed the transmit pulse-width to avoid a loss in SNR caused by target echoes that are not contained within the reference waveform.

Equal Transmit and Reference Waveform LFM Slopes. For the case where the transmit and reference waveform LFM slopes are equal ($\alpha = \alpha_R$), the IF signal is an uncoded pulse with frequency offset given by

$$\delta f = f_d + \alpha(\tau_R - \tau) \quad (8.29)$$

The frequency offset is measured using spectrum analysis and converted to target time delay and range relative to the reference waveform by

$$\begin{aligned} \Delta\tau &= \tau - \tau_R = -\frac{\delta f}{\alpha} \\ \Delta r &= (R - R_0) = \frac{c}{2} \Delta\tau \end{aligned} \quad (8.30)$$

where $R_0 = c\tau_R/2$ is the range corresponding to the time delay of the reference waveform.

Kellogg⁶⁵ describes additional considerations for application of time-domain weighting in stretch processing and provides details on compensation techniques for hardware errors. The effect of time mismatch between the signal and the weighting function is analyzed by Temes.⁶⁶

Unequal Transmit and Reference Waveform Slopes. A stretch processor with unequal frequency-slope waveforms requires pulse compression of the residual linear FM at the output of the correlation mixer. A linear FM signal with a slope of $\alpha_{in} - \alpha_R$ occurs at the target range, which is offset in frequency from the IF carrier frequency by $\alpha_R(\tau_R - \tau)$. With the range-doppler coupling of the LFM waveform, the apparent time delay of this target will be

$$\tau_{app} = -\alpha_R(\tau_R - \tau)/(\alpha - \alpha_R) \quad (8.31)$$

This result can be interpreted as yielding a time-expansion factor of $\alpha_R/(\alpha - \alpha_R)$ for the compressed pulse. As for the case of equal LFM slopes, the range window width depends on the achievable processing bandwidth.

Stretch Processing Range Resolution Width. The 6-dB frequency resolution width for spectral analysis using a rectangular window of time duration equal to the transmit pulselength is

$$\Delta f_6 = \frac{1.21}{T} \quad (8.32)$$

The 6-dB time delay resolution width obtained by stretch processing is obtained by dividing Δf_6 by $|\alpha|$ to convert to units of time delay:

$$\tau_6 = \frac{\Delta f_6}{(B/T)} = \frac{1.21}{B} \quad (8.33)$$

Consequently, the 6-dB resolution width achieved by stretch processing is the same as that achieved by the matched filter for the LFM waveform. The 6-dB range resolution width is

$$\Delta R_6 = 1.21 \frac{c}{2B} \quad (8.34)$$

Time-domain weighting is utilized in the spectral analysis processing to reduce the time sidelobes of the compressed pulse and improve the resolution performance when multiple targets are present within the range window. As an example, the use of Hamming time-domain weighting reduces the peak time sidelobe level from -13.2 dB to -42.8 dB with an increase in the 6-dB frequency resolution width to $\Delta f_6 = 1.81/T$. The 6-dB range resolution width for Hamming weighting is

$$\Delta R_6 = 1.81 \frac{c}{2B} \text{ (Hamming Weighting)} \quad (8.35)$$

Range Window Width. The width of the range window is established by the bandwidth of the spectral analysis and the LFM slope of the transmit waveform. Assume a time window of width Δt and a stretch processing bandwidth B_p . A target at the edge of the time window yields a frequency offset equal to one-half of the processing bandwidth:

$$\frac{B}{T} \frac{\Delta t}{2} = \frac{B_p}{2}$$

or

$$\Delta t = T \frac{B_p}{B} = \frac{B_p}{(B/T)} \quad (8.36)$$

The range window width is

$$\Delta r = \frac{cT}{2} \frac{B_p}{B} = \frac{c}{2} \frac{B_p}{(B/T)} \quad (8.37)$$

Stretch Pulse Compression Radar Examples. This section describes three examples of radars that employ stretch pulse compression systems.

Long Range Imaging Radar.^{62,63} The Long Range Imaging Radar (LRIR) is an X-band radar with stretch processing bandwidths of 0.8, 1.6 MHz, and 3.2 MHz. The wideband waveform has a swept bandwidth of 1000 MHz, to a pulsedwidth of approximately 250 μ s, and a LFM slope $B/T \approx 1000 \text{ MHz}/(250 \mu\text{s}) = 4 \text{ MHz}/\mu\text{s}$. The range window width for the 3.2 MHz processing bandwidth is

$$\Delta r = \frac{c}{2} \frac{B_p}{(B/T)} = \frac{150 \text{ m}/\mu\text{s} \times 3.2 \text{ MHz}}{4 \text{ MHz}/\mu\text{s}} = 120 \text{ m}$$

Millimeter Wave Radar. The stretch processing implementation for the Millimeter Wave radar (MMW) located at Kwajalein Atoll is described by Abouzahara and Avent.⁶⁴ The MMW radar operates at a carrier frequency of 35 GHz using waveforms with a maximum swept bandwidth of 1000 MHz and pulsedwidth of 50 μ s. The LFM slope for the transmit waveform is

$$\alpha = \frac{B}{T} = \frac{1000 \text{ MHz}}{50 \mu\text{s}} = 20 \text{ MHz}/\mu\text{s}$$

The stretch processing bandwidth is $B_p = 5 \text{ MHz}$. The width of the stretch processing time window is

$$\Delta t = \frac{5 \text{ MHz}}{20 \text{ MHz}/\mu\text{s}} = 0.25 \mu\text{s}$$

The reference waveform pulsedwidth is $T_R = 50 + 0.25 = 50.25 \mu\text{s}$ to avoid a loss in SNR for targets at the edges of the range window. The swept bandwidth of the reference waveform and the range window width are

$$B_R = 20 \text{ MHz}/\mu\text{s} \times 50.25 \mu\text{s} = 1005 \text{ MHz}$$

$$\Delta r = \frac{c}{2} \Delta t = 150 \text{ m}/\mu\text{s} \times 0.25 \mu\text{s} = 37.5 \text{ m}$$

The 6-dB range resolution width with Hamming weighting applied over the 50- μ s pulsedwidth in the spectral analysis processing is

$$\Delta R_6 = 1.81 \frac{c}{2B} = 1.81 \frac{150 \text{ m}/\mu\text{s}}{1000 \text{ MHz}} = 0.27 \text{ m}$$

*Cobra Dane Wideband Pulse Compression System.*⁶⁷ The characteristics of the wideband pulse compression system developed for the Cobra Dane radar are summarized in Table 8.9.

TABLE 8.9 Cobra Dane Wideband Pulse Compression System Characteristics (*adapted from Filer and Hart⁶⁷ © IEEE 1976*)

Characteristic	Value
Transmit LFM bandwidth	1175 to 1375 MHz
Reference LFM bandwidth	1665 to 1865 MHz*
Transmit waveform swept bandwidth, B	200 MHz
Reference waveform swept bandwidth, B_{ref}	200 MHz*
Transmit pulselength, T	1000 μs
Reference pulselength, T_{ref}	1000 μs*
Transmit waveform LFM slope	0.2 MHz/μs (up-chirp)
Compressed pulselength (-3 dB), τ_3	3.75 ft
Time-bandwidth product, TB	200,000
Time sidelobe level	-30 dB
Target range window	240 ft
Number of range samples	400
Range sample spacing	0.6 ft
First IF (at output of correlation mixer)	490 MHz
Second IF	60 MHz
Stretch processing bandwidth, B_p	100 kHz
A/D converter sampling frequency	1 MHz (in I and Q baseband channels)

* Excludes pulselength and swept bandwidth extension due to 240-ft range window

APPENDIX

Signal Analysis Summary.^{68–70} Table 8.10 is a summary of signal analysis definitions and relationships. Table 8.11 shows Woodward's Fourier transform rules and pairs.⁶⁹ These relationships simplify the application of signal analysis techniques. In most cases, it will not be necessary to explicitly perform an integration to evaluate the Fourier transform or inverse Fourier transform.

TABLE 8.10 Signal Analysis Definitions and Relationships

1	Fourier transform (spectrum) of signal $x(t)$	$X(f) = \int_{-\infty}^{\infty} x(t) e^{-j2\pi ft} dt$
2	Inverse Fourier transform of spectrum $X(f)$	$x(t) = \int_{-\infty}^{\infty} X(f) e^{j2\pi ft} df$
3	Convolution of signals $x(t)$ and $y(t)$	$y(t) = x(t) * h(t)$ $= \int_{-\infty}^{\infty} x(\tau) h(t - \tau) d\tau = \int_{-\infty}^{\infty} x(t - \tau) h(\tau) d\tau$
4	Filter frequency response	$H(f) = Y(f)/X(f)$
5	Euler's identity	$e^{j\theta} = \cos \theta + j \sin \theta$

TABLE 8.10 Signal Analysis Definitions and Relationships (*Continued*)

6	Cosine and sine functions expressed in terms of complex exponentials	$\cos \theta = (e^{j\theta} + e^{-j\theta})/2$
		$\sin \theta = (e^{j\theta} - e^{-j\theta})/j2$
7	Parseval's theorem (superscript asterisk indicates complex conjugate)	$\int_{-\infty}^{\infty} x(t)y^*(t)dt = \int_{-\infty}^{\infty} X(f)Y^*(f)df$
		$\int_{-\infty}^{\infty} x(t) ^2 dt = \int_{-\infty}^{\infty} X(f) ^2 df$
8	rect function	$\text{rect}(t) = \begin{cases} 1, & t < 1/2 \\ 0, & t > 1/2 \end{cases}$
9	sinc function	$\text{sinc}(f) = \sin(\pi f)/(\pi f)$
10	Repetition operator	$\text{rep}_T[x(t)] = \sum_{n=-\infty}^{\infty} x(t - nT)$
11	Comb operator	$\text{comb}_F[X(f)] = \sum_{n=-\infty}^{\infty} X(nF)\delta(f - nF)$
12	Sampling property of delta function	$\int_{-\infty}^{\infty} x(t) \delta(t - t_0)dt = x(t_0)$
13	Cauchy-Schwarz inequality	$\left \int_{-\infty}^{\infty} f(x)g(x)dx \right ^2 \leq \int_{-\infty}^{\infty} f(x) ^2 dx \int_{-\infty}^{\infty} g(x) ^2 dx$ with equality if and only if $f(x) = k_1 g^*(x)$

Radar Transmit Waveforms.^{2,68,71-73} The transmitted waveforms used in radar are bandpass signals that can be expressed in the form

$$x(t) = a(t)\cos[2\pi f_0 t + \phi(t)] \quad (8.38)$$

where $a(t)$ is the amplitude modulation (V), $\phi(t)$ is the phase modulation (rad), and f_0 is the carrier frequency (Hz). The amplitude and phase modulation functions vary slowly compared to the period of the carrier ($1/f_0$). Consequently, $x(t)$ is a narrowband waveform with a bandwidth that is small compared to the carrier frequency.

Complex Envelope. The complex envelope of $x(t)$ is given by

$$u(t) = a(t)e^{j\phi(t)} \quad (8.39a)$$

TABLE 8.11 Fourier Transform Rules and Pairs

	Signal	Spectrum	Comments
1	$x(t)$	$X(f)$	Fourier transform pair
2	$Ax(t) + Bu(t)$	$AX(f) + BU(f)$	Linearity
3	$x(-t)$	$X(-f)$	Signal time reversal
4	$x^*(t)$	$X^*(-f)$	Conjugate of signal
5	dx/dt	$j2\pi fX(f)$	Time domain differentiation
6	$-j2\pi t x(t)$	dX/df	Frequency domain differentiation
7	$x(t - \tau)$	$X(f) \exp(-j2\pi f\tau)$	Signal time shift
8	$x(t)\exp(j2\pi f_0 t)$	$X(f - f_0)$	Signal frequency shift
9	$x(t/T)$	$ T X(f/T)$	Time scaling
10	$x(t) * y(t)$	$X(f)Y(f)$	Time domain convolution
11	$x(t)y(t)$	$X(f) * Y(f)$	Time domain multiplication
12	$\text{rep}_T[x(t)]$	$ 1/T \text{comb}_{1/T}[X(f)]$	Woodward's repetition operator
13	$\text{comb}_T[x(t)]$	$ 1/T \text{rep}_{1/T}[X(f)]$	Woodward's comb operator
14	$X(t)$	$x(-f)$	Time-frequency interchange (duality)
15	$\delta(t)$	1	Delta function in time
16	1	$\delta(f)$	Delta function in frequency
17	$\text{rect}(t)$	$\text{sinc}(f)$	rect function in time
18	$\text{sinc}(t)$	$\text{rect}(f)$	rect function in frequency
19	$\exp(-\pi t^2)$	$\exp(-\pi f^2)$	Gaussian time function

The bandpass signal is expressed in terms of the complex envelope by

$$u(t) = \text{Re}[x(t)e^{j2\pi f_0 t}] \quad (8.39b)$$

Complex Envelope Representation of Radar Echoes.⁷³ The radar echo signal from a point target is

$$s_r(t) = A_r a(t - t_d) \cos[2\pi(f_0 + f_d)(t - t_d) + \phi(t - t_d)] \quad (8.40)$$

where A_r is a dimensionless amplitude scale factor, t_d is the target time delay (s), f_d is the target doppler shift (Hz), $a(t)$ is the amplitude modulation (V), $\phi(t)$ is the phase modulation (rad), and f_0 is the transmit carrier frequency (Hz). The complex envelope of $s_r(t)$ is

$$u_r(t) = A_r e^{-j2\pi f_0 t_d} u(t - t_d) e^{j2\pi f_d(t - t_d)} \quad (8.41)$$

The term $u(t - t_d)$ is the complex envelope of the transmit waveform delayed in time by t_d . The complex exponential $\exp[j2\pi f_d(t - t_d)]$ represents a linear phase modulation versus time that is impressed on the received echo signal by the doppler shift f_d . The carrier phase shift is $\theta_c = -2\pi f_0 t_d$.

The time delay and doppler shift are expressed in terms of target range and range-rate by $t_d = 2R/c$ (s) and $f_d = -(2/\lambda)V_r$ (Hz), where R is the target range (m), $V_r = dR/dt$

is the range-rate (negative for an incoming target), c is the speed of light, and $\lambda = c/f_0$ (m) is the carrier wavelength.

Matched Filters.^{2,74} A matched filter achieves maximum output signal-to-noise ratio for a signal received in white noise. The matched filter frequency response for a signal $u(t)$ is

$$H_{\text{mf}}(f) = k_1 U^*(f) e^{-j2\pi f t_1} \quad (8.42)$$

where k_1 is an arbitrary complex constant and $U(f)$ is the spectrum of $u(t)$. The time delay t_1 is required to exceed the duration of $u(t)$ to achieve a causal impulse response that is zero for negative time. The matched filter impulse response is

$$h_{\text{mf}}(t) = k_1 u^*(t_1 - t) \quad (8.43)$$

The peak signal-to-noise to mean-noise-power ratio at the output of a filter with frequency response $H(f)$ is defined as

$$(S/N)_o = \frac{A_o^2}{\sigma_{n_o}^2} \quad (8.44)$$

where A_o is the matched filter output signal amplitude at the peak of the signal and $\sigma_{n_o}^2$ is the matched filter output noise power. The matched filter output SNR is given by*

$$(S/N)_{\text{mf}} = \frac{2E}{N_0} \quad (8.45)$$

where E is the energy of the received bandpass signal at the matched filter input (J), and N_0 is the one-sided noise power spectrum at the matched filter input (W/Hz).

Filter Matching Loss. Filter matching loss L_m is the loss in SNR that results when a signal is not processed using a matched filter. The filter matching loss is defined as

$$L_m = \frac{(S/N)_{\text{mf}}}{(S/N)_o} \quad (8.46)$$

where $(S/N)_o$ is the SNR at the output of a filter with frequency response $H(f)$ and $(S/N)_{\text{mf}}$ is the matched filter SNR. The filter matching loss can also be expressed as

$$L_m = \frac{(2E/N_0)}{(S/N)_o} \quad (8.47)$$

where the matched filter SNR is given by $(S/N)_{\text{mf}} = (2E/N_0)$. The filter matching loss is ≥ 1 , where $L_m = 1$ for the matched filter. The filter matching loss expressed in decibels is $L_m(\text{dB}) = 10\log(L_m)$ and equals 0 dB for the matched filter.

* An alternate definition of signal-to-noise ratio is also used in the literature in which the signal power at the peak of the waveform is averaged over one cycle of the carrier.^{75,76} In this case, the average signal power is one-half of the peak signal power and the matched-filter output SNR is E/N_0 .

Ambiguity Functions.^{2,71,72,77–79} The autocorrelation[†] function for a transmit waveform with complex envelope $u(t)$ is defined as

$$\chi_u(\tau, f_d) = \int_{-\infty}^{\infty} u(t)u^*(t + \tau)e^{j2\pi f_d t} dt \quad (8.48)$$

where τ is the relative time delay and f_d is doppler shift. The relative time delay is positive for a target further in range than a reference target, and doppler frequency is positive for an incoming target (negative range-rate). The complex envelope $u(t)$ is normalized to unit energy

$$\int_{-\infty}^{\infty} |u(t)|^2 dt = 1 \quad (8.49)$$

The ambiguity function of $u(t)$ is defined as the square magnitude of the autocorrelation function

$$\Psi_u(\tau, f_d) = |\chi_u(\tau, f_d)|^2 \quad (8.50)$$

The ambiguity function is interpreted as a surface above the delay-doppler $(\tau - f_d)$ plane. The maximum value of the ambiguity function is unity at the origin ($\tau = f_d = 0$):

$$\Psi_u(\tau, f_d) \leq \Psi_u(0, 0) = 1 \quad (8.51)$$

The volume under the ambiguity surface is unity for any waveform $u(t)$:

$$\int_{-\infty}^{\infty} \int_{-\infty}^{\infty} \Psi_u(\tau, f_d) d\tau df_d = 1 \quad (8.52)$$

In the general case, where the energy of the complex envelope is not normalized to unity, the value of the ambiguity function at the origin is equal to $(2E)^2$ where E is the energy of the bandpass signal corresponding to $u(t)$, and the volume under the ambiguity function is also equal to $(2E)^2$. The normalization condition is equivalent to the assumption that the energy of the bandpass transmit waveform equals 0.5 J.

Matched Filter Time Response. The matched filter time response to a target with doppler shift f_d can be expressed in terms of the autocorrelation function. The matched filter impulse response with $k_1 = 1$ and $t_1 = 0$ is

$$h_{\text{mf}}(t) = u^*(-t) \quad (8.53)$$

The matched filter input signal is assumed to have zero time delay and a doppler shift f_d :

$$s(t) = u(t)e^{j2\pi f_d t} \quad (8.54)$$

[†] The terminology for this function is not standardized in the literature. Woodward⁶⁹ uses the term correlation function. The term time-frequency autocorrelation function is used by Spafford.⁸⁰ The signs associated with τ and f_d within the integrand also differ in the literature. The standardized definition proposed by Sinsky and Wang⁷⁸ is used in this chapter.

The matched filter output signal $y(t)$ is found by convolution of $s(t)$ with the matched filter impulse response $h_{mf}(t)$:

$$y(t) = \int_{-\infty}^{\infty} u(t') u^*(t' - t) e^{j2\pi f_d t'} dt' \quad (8.55)$$

Comparison of this result with the definition of the autocorrelation function shows that the matched filter response can be expressed as

$$y(t) = X_u(-t, f_d) \quad (8.56)$$

As a result, the matched filter time response for a target with doppler frequency f_d is a time-reversed version of the autocorrelation function.

Conditions for Target Resolution in Time Delay and Doppler Frequency.^{72,78} Assume that two targets with equal radar cross sections are present at the same angular position. The first target (termed the *reference target*) is located at the origin of the delay-doppler plane with zero relative time delay and zero doppler frequency, and the second target is at relative time delay τ and doppler frequency f_d . The relative time delay is positive when the second target is farther in range than the reference target and the doppler frequency is positive for an incoming target. The matched-filter output power for the reference target is proportional to the ambiguity function and is given by

$$P_{\text{ref}} = \Psi_u(0,0) = 1 \quad (8.57)$$

The matched filter output power for the second target, evaluated at the peak of the reference target, is

$$P_2 = \Psi_u(\tau, f_d) \quad (8.58)$$

The second target is unresolved from the reference target at locations in the delay-doppler plane where $\Psi_u(\tau, f_d) \approx 1$.

REFERENCES

1. J. R. Klauder, A. C. Price, S. Darlington, and W. J. Albersheim, "The theory and design of chirp radars," *Bell Syst. Tech. J.*, vol. 39, pp. 745–808, July 1960.
2. C. E. Cook and M. Bernfield, *Radar signals: An Introduction to Theory and Application*, New York: Academic Press, 1967.
3. C. E. Cook and J. Paolillo, "A pulse compression predistortion function for efficient sidelobe reduction in a high-power radar," *Proc. IEEE*, pp. 377–389, April 1964.
4. T. T. Taylor, "Design of line-source antennas for narrow beamwidth and low sidelobes," *IRE Trans.*, vol. AP-3, pp. 16–28, January 1955.
5. R. C. Hansen, "Aperture theory," in *Microwave Scanning Antennas*, vol. I, R. C. Hansen (ed.), New York: Academic Press, 1964, chap. 1.
6. H. Gautier and P. Tournois, "Signal processing using surface-acoustic-wave and digital components," *IEEE Proc.*, vol. 127, pt. F, pp. 92–93, April 1980.
7. A. J. Slobodnik, Jr., "Surface acoustic waves and SAW materials," *Proc. IEEE*, vol. 64, pp. 581–594, May 1976.
8. T. W. Bristol, "Acoustic surface-wave-device applications," *Microwave J.*, vol. 17, pp. 25–27, January 1974.

9. J. W. Arthur, "Modern SAW-based pulse compression systems for radar applications," *Electronics & Communications Engineering Journal*, December 1995.
10. R. C. Williamson, "Properties and applications of reflective-array devices," *Proc. IEEE*, vol. 64, pp. 702–703, May 1976.
11. G. W. Judd, "Technique for realizing low time sidelobe levels in small compression ratio chirp waveforms," *Proc. IEEE Ultrasonics Symp.*, 1973, pp. 478–481.
12. A. Pohl, C. Posch, F. Seifert, and L. Reindl, "Wideband compressive receiver with SAW convolver," *1995 IEEE Ultrasonics Symposium*, pp. 155–158.
13. X. Shou, J. Xu, H. Wang, and Q. Xu, "SAW pulse compression systems with lower sidelobes," *1997 Asia Pacific Microwave Conference*, pp. 833–835.
14. T. Murakami, "Optimum waveform study for coherent pulse doppler," *RCA Final Rept.*, prepared for Office of Naval Research, Contract Nonr 4649(00)(x), AD641391, February 28, 1965.
15. T. Collins and P. Atkins, "Nonlinear frequency modulation chirps for active sonar," *IEE Proc.-Radar, Sonar Navig.*, vol. 146, no. 6, pp. 312–316, December 1999.
16. L. R. Varschney and D. Thomas, "Sidelobe reduction for matched range processing," *2003 IEEE Radar Conference*, pp. 446–451.
17. N. Levanon and E. Mozeson, *Radar Signals*, New York: IEEE Press, John Wiley & Sons, Inc., 2004, pp. 106, 145.
18. R. H. Barker, "Group synchronization of binary digital systems," in *Communication Theory*, W. Jackson (ed.), New York: Academic Press, 1953, pp. 273–287.
19. P. J. Edmonson, C. K. Campbell, and S. F. Yuen, "Study of SAW pulse compression using 5×5 Barker codes with quadriphase IDT geometries," *1988 IEEE Ultrasonics Symposium*, pp. 219–222.
20. T. Felhauer, "Design and analysis of new P(n,k) polyphase pulse compression codes," *IEEE Transactions on Aerospace and Electronics Systems*, vol. 30, no. 3, pp. 865–874, July 1994.
21. R. Turyn and J. Stover, "On binary sequences," *Proc. Am. Math. Soc.*, vol. 12, pp. 394–399, June 1961.
22. D. G. Luenburger, "On Barker codes of even length," *Proc. IEEE*, vol. 51, pp. 230–231, January 1963.
23. R. Turyn, "On Barker codes of even length," *Proc. IEEE* (correspondence), vol. 51, p. 1256, September 1963.
24. L. Bömer and M. Antweiler, "Polyphase Barker sequences," *Electronics Letters*, vol. 23, no. 23, pp. 1577–1579, November 9, 1989.
25. H. Meikle, *Modern Radar Systems*, Norwood, MA: Artech House, 2001, p. 258.
26. B. L. Lewis, "Range-time-sidelobe reduction technique for FM-derived polyphase PC codes," *IEEE Transactions on Aerospace and Electronics Systems*, vol. 29, no. 3, pp. 834–863, July 1993.
27. W. W. Peterson and E. J. Weldon, Jr., *Error Correcting Codes*, Cambridge: M.I.T. Press, 1972, app. C.
28. M. I. Skolnik, *Introduction to Radar Systems*, 3rd Ed., New York: McGraw Hill, 2001, p. 367.
29. N. Levanon and E. Mozeson, *Radar Signals*, New York: IEEE Press, John Wiley & Sons, Inc., 2004, pp. 106–109.
30. L. Bömer and M. Antweiler, "Polyphase Barker sequences," *Electronics Letters*, vol. 25, no. 23, pp. 1577–79, November 9, 1989.
31. W-D. Wirth, *Radar Techniques Using Array Antennas*, IEE Radar, Sonar, Navigation and Avionics Series 10, London: The Institution of Electrical Engineers, 2001.
32. R. L. Frank, "Polyphase codes with good nonperiodic correlation properties," *IEEE Trans.*, vol. IT-9, pp. 43–45, January 1963.
33. B. L. Lewis and F. F. Kretschmer, Jr., "A new class of polyphase pulse compression codes and techniques," *IEEE Trans.*, vol. AES-17, pp. 364–372, May 1981. (See correction, *IEEE Trans.*, vol. AES-17, p. 726, May 1981.)
34. B. L. Lewis, "Range-time-sidelobe reduction technique for FM-derived polyphase PC codes," *IEEE Transactions on Aerospace and Electronics Systems*, vol. 29, no. 3, pp. 834–863, July 1993.

35. B. L. Lewis and F. F. Kretschmer, Jr., "Linear Frequency Modulation Derived Polyphase Pulse Compression Codes," *IEEE Trans. on Aerospace and Electronics Systems*, AES-18, no. 5, pp. 636–641, September 1982.
36. J. W. Taylor and H. J. Blinchikoff, "Quadriphase code-a radar pulse compression signal with unique characteristics," *IEEE Trans. Aerospace and Electronic Systems*, vol. 24, no. 2, pp. 156–170, March 1988.
37. H. J. Blinchikoff, "Range sidelobe reduction for the quadriphase codes," *IEEE Trans. Aerospace and Electronic Systems*, vol. 32, no. 2, April 1996, pp. 668–675.
38. N. Levanon, "Stepped-frequency pulse-train radar signal," *IEE Proc-Radar Sonar Navigation*, vol. 149, no. 6, December 2002.
39. A. W. Rihaczek, *Principles of High-Resolution Radar*, New York: McGraw-Hill Book Company, 1969, chap. 8.
40. J. P. Donohue and F. M. Ingels, "Ambiguity function properties of frequency hopped radar/sonar signals," *Proc. of the 1989 Southeastcon*, session 10B6, pp. 85–89.
41. J. P. Costas, "A study of a class of detection waveforms having nearly ideal range-doppler ambiguity properties," *Proc. of the IEEE*, vol. 72, no. 8, August 1984.
42. B. R. Mahafza, *Radar Systems Analysis and Design using MATLAB*, 2000, Boca Raton: Chapman & Hall/CRC, 2000.
43. B. M. Popvik, "New construction of Costas sequences," *Electronic Letters*, vol. 25, no. 1, January 5, 1989.
44. M. I. Skolnik, *Introduction to Radar Systems*, 3rd Ed., New York: McGraw Hill, 2001, pp. 355–57.
45. D. P. Morgan, "Surface acoustic wave devices and applications," *Ultrasonics*, vol. 11, pp. 121–131, 1973.
46. L. O. Eber and H. H. Soule, Jr., "Digital generation of wideband LFM waveforms," *IEEE Int. Radar Conf. Rec.*, 1975, pp. 170–175.
47. AD9858 1-GSPS direct digital synthesizer data sheet, Rev. A, 2003, Analog Devices, Norwood, MA (available at www.analog.com).
48. J. K. Hartt and L. F. Sheats, "Application of pipeline FFT technology in radar signal and data processing," *EASCON Rec.*, 1971, pp. 216–221; reprinted in David K. Barton, *Radars*, vol. 3, Ann Arbor: Books on Demand UMI, 1975.
49. P. E. Blankenship and E. M. Hofstetter, "Digital pulse compression via fast convolution," *IEEE Trans. on Acoustics, Speech and Signal Processing*, vol. ASSP-23, no. 2, pp. 189–222, April 1975.
50. L. W. Martinson and R. J. Smith, "Digital matched filtering with pipelined floating point fast Fourier transforms (FFTs)," *IEEE Trans. on Acoustics, Speech and Signal Processing*, vol. ASSP-23, no. 2, pp. 222–234, April 1975.
51. L. E. Pellon, "A double Nyquist digital product detector for quadrature sampling," *IEEE Trans. on Signal Processing*, vol. 40, no. 7, pp. 1670–1680.
52. G. A. Shaw and S. C. Pohlig, "I/Q baseband demodulation in the RASSP SAR benchmark," Project Report RASSP-4, Massachusetts Institute of Technology, Lincoln Laboratory, 25 August 1995, <http://www.ll.mit.edu/llrassp/documents.html>.
53. M. A. Richard, "Digital I/Q," Section 3.7.3 in *Fundamentals of Radar Signal Processing*, New York: McGraw-Hill, 2005.
54. L. R. Rabiner and B. Gold, *Theory and Application of Digital Signal Processing*, Englewood Cliffs, NJ: Prentice-Hall, Inc., 1975, chap. 2.
55. J. J. Gostin, "The GE592 solid-state radar," *IEEE EASCON 1980*, pp. 197–203.
56. E. L. Cole, P. A DeCesare, M. J. Martineaus, R. S. Baker, and S. M. Buswell, "ASR-12: A next generation solid-state air traffic control radar," *IEEE 1998 Radar Conference*, pp. 9–14.
57. W. J. Caputi, Jr., "Stretch: A time-transformation technique," *IEEE Trans.*, vol. AES-7, pp. 269–278, March 1971.
58. W. J. Caputi, "A technique for the time-transformation of signals and its application to directional systems," *The Radio and Electronic Engineer*, pp. 135–142, March 1965.

59. W. J. Caputi, "Swept-heterodyne apparatus for changing the time-bandwidth product of a signal," U.S. Patent 3283080, November 1, 1966.
60. W. J. Caputi, "Pulse-type object detection apparatus," U.S. Patent, November 21, 1967.
61. K. R. Roth, M. E. Austin, D. J. Frediani, G. H. Knittel, and A. V. Mrstik, "The Kiernan reentry measurements system on Kwajalein Atoll," *The Lincoln Laboratory Technical Journal*, vol. 2, no. 2, 1989.
62. D. R. Bromaghim and J. P. Perry, "A wideband linear fm ramp generator for the long-range imaging radar," *IEEE Trans. Microwave Theory and Techniques*, vol. MTT-26, no. 5, pp. 322–325, May 1978.
63. G. R. Armstrong and M. Axelbank, "Description of the long-range imaging radar," Project Report PSI-85, Massachusetts Institute of Technology, Lincoln Laboratory, November 16, 1977.
64. M. D. Abouzahra and R. K. Avent, "The 100-kW millimeter-wave radar at the Kwajalein Atoll," *IEEE Antennas and Propagation Magazine*, vol. 36, no. 2, pp. 7–19, April 1994.
65. W. C. Kellogg, "Digital processing rescues hardware phase errors," *Microwaves & RF*, pp. 63–67, 80, November 1982.
66. C. L. Temes, "Sidelobe suppression in a range channel pulse-compression radar," *IRE Trans.*, vol. MIL-6, pp. 162–169, April 1962.
67. E. Filer and J. Hartt, "COBRA DANE wideband pulse compression system," *IEEE EASCON '76*, 1976, pp. 61-A–61-M.
68. S. Stein and J. J. Jones, "Modern Communication Principles with Application to Digital Signaling," New York: McGraw-Hill, 1967.
69. P. M. Woodward, *Probability and Information Theory with Application to Radar*, Pergamon Press, 1960.
70. D. Brandwood, "Fourier Transforms," in *Radar and Signal Processing*, Boston: Artech House, 2003.
71. G. W. Deley, "Waveform design," in *Radar Handbook*, M. I. Skolnik (ed.), 1st Ed., New York: McGraw-Hill, 1970.
72. A. I. Sinsky, "Waveform selection and processing" in *Radar Technology*, E. Brookner (ed.), Boston: Artech House, 1977, Chap. 7.
73. C. W. Helstrom, *Statistical Theory of Signal Detection*, 2nd Ed., Pergamon Press, 1968.
74. G. L. Turin, "An introduction to matched filters," *IRE Trans. Inform. Theory*, vol. IT-6, pp. 311–329, June 1960.
75. D. K. Barton, *Modern Radar System Analysis and Modeling*, Canton, MA: Artech House Inc, 2005, Chap. 5, p. 197.
76. F. E. Nathanson, J. P. Reilly, and M. N. Cohen, *Radar Design Principles: Signal Processing and the Environment*, 2nd Ed. New York: McGraw-Hill, 1991. chap. 8, p. 357.
77. A. W. Rihaczek, "Radar signal design for target resolution," *Proc. IEEE*, vol. 53, pp. 116–128, February 1965.
78. A. I. Sinsky and C. P. Wang, "Standardization of the definition of the ambiguity function," *IEEE Trans. Aerospace and Electronic Systems*, pp. 532–533, July 1974.
79. IEEE standard radar definitions, IEEE Std 686-1990, The Institution of Electrical and Electronic Engineers, New York, NY, 1990. The ambiguity function is defined on page 55 using the standardized definition given by Sinsky and Wang.
80. L. J. Spafford, "Optimum radar signal processing in clutter," *IEEE Trans. Information Theory*, vol. IT-14, no. 5, pp. 734–743, September 1968.